

Oxygen and sulfur mass-independent isotopic signatures in black crusts: the complementary negative $\Delta^{33}\text{S}$ -reservoir of sulfate aerosols?

5 Isabelle Genot^{1,2}, David Au Yang^{1,3,4}, Erwan Martin², Pierre Cartigny¹, Erwann Legendre^{2,5}, Marc De Rafelis⁶

¹Institut de physique du globe de Paris, Université de Paris, CNRS, F-75005 Paris, France.

²Sorbonne Université, CNRS-INSU, Institut des Sciences de la Terre de Paris, IsteP UMR7193 Paris, France.

10 ³GEOTOP/Université du Québec à Montréal, Montréal H3C 3P8, Canada

⁴Department of Earth and Planetary Sciences, McGill University, Montréal, Canada.

⁵LATMOS-IPSL - Sorbonne Université - Université Versailles St.-Quentin, Paris, France.

⁶GET, Université Paul Sabatier, Toulouse, France.

15 *Correspondence to:* Isabelle Genot (genot@ipgp.fr)

Abstract To better understand the formation and the oxidation pathways leading to gypsum-forming “black crusts” and investigate their bearing on the whole atmospheric SO₂ cycle, we measured the oxygen ($\delta^{17}\text{O}$, $\delta^{18}\text{O}$ and $\Delta^{17}\text{O}$) and sulfur ($\delta^{33}\text{S}$, $\delta^{34}\text{S}$, $\delta^{36}\text{S}$, $\Delta^{33}\text{S}$ and $\Delta^{36}\text{S}$) isotopic compositions of black crust sulfates sampled on carbonate building stones along a NW-SE cross-section in the Parisian Basin. The $\delta^{18}\text{O}$ and $\delta^{34}\text{S}$, ranging between 7.5 and 16.7 ± 0.5 ‰ (n = 27, 2 σ) and between -2.66 and 13.99 ± 0.20 ‰ respectively, show anthropogenic SO₂ as the main sulfur source (from ~ 2 to 81 %, average ~ 30 %) with host-rock sulfates making the complement. This is supported by $\Delta^{17}\text{O}$ -values (up to 2.6 ‰, in average ~ 0.86 ‰), requiring > 60 % of atmospheric sulfates in black crusts. Both negative $\Delta^{33}\text{S}$ - $\Delta^{36}\text{S}$ -values between -0.34 and 0.00 ± 0.01 ‰ and between -0.76 and -0.22 ± 0.20 ‰ respectively were measured in black crust sulfates, that is typical of a magnetic isotope effect that would occur during the SO₂ oxidation on the building stone, leading to ³³S-depletion in black crust sulfates and subsequent ³³S-enrichment in residual SO₂. Except for a few samples, sulfate aerosols have mostly $\Delta^{33}\text{S} > 0$ ‰ and no processes can yet explain this enrichment, resulting in a non-consistent S-budget: black crust sulfates could well represent the complementary negative $\Delta^{33}\text{S}$ -reservoir of the sulfate aerosols solving the atmospheric SO₂ budget.

1. Introduction

The oxidation of sulfur dioxide emitted into the atmosphere (between 100 and 110 Tg(SO₂).yr⁻¹, Klimont et al., 2013) can result in the formation of H₂SO₄ that forms sulfate aerosols; having light-scattering properties that alter the radiative balance of the planet. Furthermore, they also modify the microphysical properties of clouds through the number and size of cloud condensation nucleus process (CCN; e.g. (Weber et al., 2001). Although quantified with large uncertainties, the formation of sulfate aerosols results in an Earth surface cooling (Forster et al., 2007), with a negative radiative forcing from -0.62 to -0.21 W.m⁻², in average ~ -0.41 W.m⁻². Overall, sulfate aerosols are the most efficient particles that counterbalance the greenhouse effect (Stocker, 2014). Uncertainties regarding the formation of sulfate aerosols relate to the large variety of oxidants and conditions (e.g. pH) but in view of their major impact on climate, a more accurate understanding of the formation of these particles is necessary.

Primary sulfate aerosols consist of sulfates formed during their emission into the atmosphere (e.g. sea-salt sulfates, combustion products, volcanic sulfates) which involves therefore a local origin (Holt and Kumar, 1991).

45 Secondary sulfate aerosols are formed later in the atmosphere following various oxidation pathways (e.g. oxidation via OH, O₂-Transition Metal Ion (TMI), O₃, H₂O₂, NO₂...) and relate to a local or more distant sulfur source (Seinfeld and Pandis, 2016). SO₂-oxidation can occur in the gas phase (homogeneous reaction, e.g. with OH), in the aqueous phase (e.g. with H₂O₂, O₃, O₂-TMI) or on a surface (heterogeneous reaction), resulting in different size and number of aerosols particles with distinct effects on radiative balance.

50 Stable isotope geochemistry is a central tool to both characterizing sulfur sources and quantify the different oxidants. The δ notation used here is defined as:

$$\delta = [(R / R_{\text{std}}) - 1]$$

with $R = {}^{18}\text{O}, {}^{17}\text{O} / {}^{16}\text{O}$ for $\delta^{18}\text{O}$ and $\delta^{17}\text{O}$ or $R = {}^{34}\text{S}, {}^{33}\text{S}, {}^{36}\text{S} / {}^{32}\text{S}$ for $\delta^{34}\text{S}$, $\delta^{33}\text{S}$ and $\delta^{36}\text{S}$ and isotope fractionation factors are expressed as follows:

$${}^{18/16}\alpha_{\text{A-B}} = ({}^{18}\text{O}/{}^{16}\text{O})_{\text{A}} / ({}^{18}\text{O}/{}^{16}\text{O})_{\text{B}}$$

with A and B being two different phases.

55 Given that the oxidants have distinct $\delta^{18}\text{O}$ and $\Delta^{17}\text{O}$ signatures, the SO₂ oxidation pathways are commonly constrained using oxygen-multi isotope ratios ($\delta^{18}\text{O}$, $\delta^{17}\text{O}$ and $\Delta^{17}\text{O}$, defined in the following section) (Alexander et al., 2012; Bindeman et al., 2007; Jenkins and Bao, 2006; Lee and Thiemens, 2001; Savarino et al., 2000; Martin, 2018). Sulfur isotope fractionation during SO₂ oxidation by OH, O₂-TMI, H₂O₂, O₃ (Harris et al., 2012a; Harris et al., 2012b; Harris et al., 2013a; Harris et al., 2013b) and NO₂ (Au Yang et al., 2018) have been

60 determined, so additional constraints can also be brought by S-multi isotopic compositions ($\delta^{34}\text{S}$, $\delta^{33}\text{S}$, $\delta^{36}\text{S}$, $\Delta^{33}\text{S}$ and $\Delta^{36}\text{S}$). At present, it is however difficult to reach a consistent budget for tropospheric SO₂ oxidation (chemically and isotopically). Indeed, most of rural and urban sulfate aerosols have positive $\Delta^{33}\text{S}$ -values (Au Yang et al., 2019; Guo et al., 2010; Han et al., 2017; Lin et al., 2018b; Romero and Thiemens, 2003; Shaheen et al., 2014), implying either a source of SO₂ with $\Delta^{33}\text{S} > 0$ ‰ (which has not been identified yet as all known

65 sources have $\Delta^{33}\text{S} \sim 0$ ‰; (Lin et al., 2018b) or more likely processes such as SO₂ photolysis in the stratosphere (e.g. Farquhar et al. (2001), contributing to the ³³S-enriched tropospheric sulfate reservoir from initial SO₂ with $\Delta^{33}\text{S} = 0$ ‰, that should be balanced by a ³³S-depleted reservoir, but which remain scarce (see Shaheen et al., 2014; Han et al., 2017; Lin et al., 2018a). Negative $\Delta^{33}\text{S}$ -values were suggested to result specifically from combustion (Lee et al., 2002) and/or OCS-photolysis (Lin et al., 2011). Still, the mass balance among positive

70 and negative $\Delta^{33}\text{S}$ -values is not consistent. As none of the most significant tropospheric SO₂ oxidation reaction can either account for $\Delta^{33}\text{S}$ anomalies in sulfate aerosols (Au Yang et al., 2018; Guo et al., 2010; Han et al., 2017; Harris et al., 2013b; Lee et al., 2002; Lin et al., 2018a; Lin et al., 2018b; Romero and Thiemens, 2003; Shaheen et al., 2014), this leads to the suggestion that either some reactions or SO₂ sources have been overlooked. Finally, a recent study highlights the possibility of SO₂ oxidation on mineral dust surfaces resulting in ³³S-depleted sulfate

75 deposit in rural environment and subsequent ³³S-enrichment of residual SO₂ transported to cities (Au Yang et al., 2019), but the negative $\Delta^{33}\text{S}$ -values were still missing.

In this respect, black crusts potentially represent new ways to sample the atmosphere in urban regions at relatively global scale. They are generally formed by the sulfation of the underlying carbonate substrate resulting in a gypsum layer (Camuffo, 1995)(Fig. 1). Due to their degradation effects of monuments and buildings, in

80 particular because the molar volume of CaSO₄ is larger than that of CaCO₃, several studies investigated sources of sulfur in black crusts, using primarily the isotopic composition of sulfur ($\delta^{34}\text{S}$) and oxygen ($\delta^{18}\text{O}$), microscopic

and mineralogical aspects. Anthropogenic sulfur was found to be the major source contributing to monuments degradation in several localities compared to marine or volcanic sulfate sources (Longinelli and Bartelloni, 1978; Montana et al., 2012; Montana et al., 2008; Torfs et al., 1997). Sulfates from the host-rock, i.e. plaster, mortar or oxidized pyrite (defined as intrinsic in the literature; Klemm and Siedel, 2002; Kloppmann et al., 2011; Kramar et al., 2011; Vallet et al., 2006) and sulfates from aquifer rising by capillarity (Kloppmann et al., 2014) were also identified as sulfur sources in black crusts. Black crusts being sometimes the host of microbial activity (Gaylarde et al., 2007; Sáiz-Jiménez, 1995; Scheerer et al., 2009; Schiavon, 2002; Tiano, 2002), other studies investigated the role of bacteria in gypsum formation through sulfate reduction and/or SO₂ oxidation (Tiano, 2002; Tiano et al., 1975). Except the work of Šrámek (1980) measuring black crust sulfates δ³⁴S that rule out the implication of micro-organisms in their formation, no further constraint has been brought so far. In this paper, we present new oxygen and sulfur isotopic composition measurements of sulfate extracted from black crusts and report significant Δ¹⁷O, Δ³³S, Δ³⁶S anomalies that help to discuss oxygen and sulfur isotopic variations both in term of source effects to elucidate their origin and in term of fractionation processes leading to black crusts formation in the Paris area.

2. Mass-dependent and independent fractionations

As many chemical reactions, O- and S-isotopic compositions of SO₂ vary during its oxidation. Most reactions are “mass-dependent”, meaning the isotopic fractionation relies on the mass differences between the isotopes; this remains valid for most unidirectional (kinetic) and/or exchange (equilibrium) reactions. In a system with at least three isotopes, mass fractionation law at equilibrium and high temperature can be derived from their partition function (Bigeleisen and Mayer, 1947; Dauphas and Schauble, 2016; Urey, 1947; Young et al., 2002) as follows for instance with oxygen isotopes and SO₂ oxidation in sulfates:

$$^{17/18}\beta_{\text{SO}_4\text{-SO}_2} = \ln^{17/16}\alpha_{\text{SO}_4\text{-SO}_2} / \ln^{18/16}\alpha_{\text{SO}_4\text{-SO}_2} \sim (1/m_{16} - 1/m_{17}) / (1/m_{16} - 1/m_{18}) \sim 0.5305$$

with ¹⁷β_{SO₄-SO₂, the mass exponent describing the relative fractionation between ¹⁷O/¹⁶O and ¹⁸O/¹⁶O, m, the mass of each isotope and ^{17/16}α_{SO₄-SO₂, the isotope fractionation factor between two phases (defined in the introduction). Same equations can be written for ³³S and ³⁶S.}}

Here, we will use ¹⁷β, ³³β and ³⁶β-values ~ 0.5305, 0.515 and 1.889 respectively, the high-temperature limit, which has been shown to be applicable for a wide range of temperature phases (Dauphas and Schauble, 2016) and isotope systems (S, Fe, Mg, O, Si...). Thus, the β-exponent represents the slope in a δ-δ space, called the “mass-dependent fractionation line”, which is actually approximated from a curve (this simplification is not used in this paper). Deviations from the reference “mass-dependent” curve do not imply necessarily isotopic variations that are independent from the isotopes masses. These deviations are quantified with the Δ-parameter expressed following Eq. (1), Eq. (2) and Eq. (3) (Farquhar and Wing, 2003; Thiemens, 1999):

$$\Delta^{17}\text{O} = \delta^{17}\text{O} - 1000 \times [(\delta^{18}\text{O} / 1000 + 1)^{0.5305} - 1] \quad (1)$$

$$\Delta^{33}\text{S} = \delta^{33}\text{S} - 1000 \times [(\delta^{34}\text{S} / 1000 + 1)^{0.515} - 1] \quad (2)$$

$$\Delta^{36}\text{S} = \delta^{36}\text{S} - 1000 \times [(\delta^{34}\text{S} / 1000 + 1)^{1.889} - 1] \quad (3)$$

Small non-zero Δ¹⁷O-Δ³³S-Δ³⁶S-values (typically between - 0.1 and + 0.1 ‰) can result from mixing, mass-dependent processes such as Rayleigh distillation or mass conservation effects and non-equilibrium processes (Farquhar et al., 2007; Ono et al., 2006) whereas large non-zero Δ¹⁷O-Δ³³S-Δ³⁶S-values (higher than + 0.2 ‰ or

lower than - 0.2 ‰) imply mass-independent fractionation (Cabral et al., 2013; Delavault et al., 2016; Farquhar et al., 2000; Farquhar et al., 2007b; Farquhar et al., 2002; Ono et al., 2003). Oxidation reactions would then change $\delta^{17}\text{O}$ and $\delta^{18}\text{O}$ but not the $\Delta^{17}\text{O}$, which would primarily vary through mixing of O-reservoirs with variable $\Delta^{17}\text{O}$. Possible mechanisms producing non-zero $\Delta^{17}\text{O}$ - $\Delta^{33}\text{S}$ - $\Delta^{36}\text{S}$ -values recorded in sulfate aerosols are discussed in the following sections. In this paper, we investigate the different processes responsible for the $\Delta^{17}\text{O}$, $\Delta^{33}\text{S}$ and $\Delta^{36}\text{S}$ recorded by black crust sulfates and what can be inferred in terms of black crust formation.

3. Sampling and Methods

3.1. Sampling sites

To access sulfate aerosols from the Parisian region, black crusts were sampled following the prevailing winds according to a NW-SE cross-section, from Fécamp to Sens (Fig. 2 b, c). Therefore, the studied area covers rural, urban and industrial zones including four power plants, major highways and the large Paris metropolis.

A total of 27 samples were collected on the external face of churches, monuments and on walls in the streets. The substrates were generally Lutetian and Cretaceous limestone, the typical building rocks in the Parisian Basin. To ensure a representative sample of sulfate aerosols, the sampling was carried out preferentially oriented to NW or, if possible, not directly exposed to traffic emission. Moreover, to avoid sulfate contamination from soils (i.e. salts by capillary action, water from run-off...), black crusts were sampled at least at a height of 1.50 m above ground level. More details about samples are summarized in Table 1.

3.2 Methods

X-ray diffractometry (XRD D2-phaser BRUCKER, IStEP Sorbonne Université) was used to specify the mineralogical nature of each sample and therefore, to demonstrate the nature of sulfur. Structural and chemical aspects were subsequently investigated using Scanning Electron Microscopy (SEM, IStEP Sorbonne Université). Sulfates were leached from 20-100 mg of black crusts and the conversion of gypsum into pure barite was performed according to the protocol developed at the Institut des Sciences de la Terre de Paris (IStEP) as described by Le Gendre et al. (2017). The use of an ion-exchange resin in this protocol enables the concentration and separation of sulfates from other compounds such as nitrates that can affect the O-isotopic measurements. From about 3 mg of the pure barite samples, the sulfate O-isotopic ratios were measured using the laser fluorination line coupled to a Delta V IR-MS at the Institut de Physique du Globe de Paris (IPGP) (Bao and Thiemens, 2000). Due to SO_2F_2 formation during BaSO_4 fluorination, that leads to incomplete O_2 extraction, measured $\delta^{18}\text{O}$ and $\delta^{17}\text{O}$ are fractionated but were corrected as deduced from the analysis of the international barite standard NBS127 ($\delta^{18}\text{O} = 8.6$ ‰, $\Delta^{17}\text{O} \sim 0$ ‰); no correction was applied on $\Delta^{17}\text{O}$, remaining unchanged (Bao and Thiemens, 2000). For two NBS127 measured each day during five days ($n=10$), we obtained a mean $\delta^{18}\text{O} = -0.43 \pm 0.54$ (2σ) and a mean $\Delta^{17}\text{O} = 0.044 \pm 0.020$ (2σ) within error of the recent value reported by Cowie and Johnston (2016). Bao (2006) reported up to 2‰ variation in the correction factor that would result from sample impurity but as our samples were purified with an ion-exchange resin and that the mean variation of the duplicates is lower than for NBS127, we applied a correction factor of 9.03 on $\delta^{18}\text{O}$ for all analyzed samples based on the certified value of NBS127.

160 The remaining BaSO₄ was reduced to hydrogen sulfide (H₂S) by reaction for 2 hours with a heated mixture of
hydrochloric (HCl), hydroiodic (HI) and hypophosphorous (H₃PO₂) acids following the protocol described in
Thode et al. (1961). H₂S was purged and precipitated as silver sulfide (Ag₂S) passing through a silver nitrate
(AgNO₃) solution. Ag₂S was then converted to SF₆ and purified (Ono et al., 2006b) and quantified before being
165 analyzed by isotope ratio mass spectrometry (Thermo-Fisher MAT-253) at McGill University. The δ³⁴S-values
are expressed versus V-CDT assuming a δ³⁴S_{S1} = -0.30 ‰ vs CDT isotope composition. Our data were then
expressed against CDT following the method described by Defouilloy et al. (2016). Analysis of the IAEA-S1 in
the laboratory yielded: δ³⁴S = -0.30 ‰, Δ³³S = 0.09 ‰ and Δ³⁶S = -0.70 ‰ vs V-CDT. Analysis of the IAEA-S3
(n = 8) gave: δ³⁴S = -32.44 ± 0.30 ‰, Δ³³S = 0.069 ± 0.023 ‰ and Δ³⁶S = -0.970 ± 0.277 ‰ vs V-CDT. All
values are within the ranges of δ³⁴S, Δ³³S, Δ³⁶S accepted or measured by other laboratories for these international
170 standards (Au Yang et al., 2016; Farquhar et al., 2007b; Labidi et al., 2014; Ono et al., 2006b; Geng et al., 2019).

4. Results

4.1. Morphological and chemical aspects

175 After having confirmed the gypsum nature of the sample by X-ray diffraction, the structural and chemical aspects
of black crusts from four different environments were investigated on the basis of SEM observations. In
agreement with previous studies (Fronteau et al., 2010; Siegesmund et al., 2007), all samples display two distinct
layers. An opaque layer (few tens of μm) comprising massive and sparse gypsum crystals as well as aggregates of
clay minerals and particulate matter overlying a layer (~100 μm) composed of more crystallized acicular and
180 rosette-like crystals gypsum (tens of μm, Fig. 3a). As shown on Fig. 3b, soot is both present in urban and rural
encrustations being consistent with previous observations (Guo et al., 2010). Moreover, fly ash particles resulting
from coal or oil combustion are present in all environments. Parisian samples (PA13-2 and PA14-1) show many
fly ashes of a diameter size < 10 μm (primarily composed of Fe) with small gypsum crystals (few micrometers)
on their surfaces (Fig. 3c). This is consistent with the catalyzer effect of combustion particles released by diesel
185 and gasoline vehicles, which increases the rate of SO₂ fixation as sulfate (Rodriguez-Navarro and Sebastian,
1996). Scarce fly ashes were also observed in samples from the city of Mantes-la-Jolie (northwest of Paris). The
sample MR27-1 shows isolated halite crystals (< 10 μm, Fig. 3e), which can result from marine aerosols, in
agreement with its location near the sea as well as numerous fly ashes (Fig. 3d), most likely from power plants
and traffic roads. The dissolution of rhomboedric calcite and subsequent precipitation of gypsum crystals is also
190 illustrated on Fig. 3f.

In summary, the presence of particulate matter and salts highlights several local or distant sources of S-bearing
compounds and a prevailing anthropogenic source in the whole Parisian Basin atmosphere, which may be
distinguished and quantified with the isotopic composition of sulfate.

195

4.2. Isotopic composition of black crusts sulfates

The sulfur and oxygen isotopic compositions of black crust sulfates are reported in Table 2. The δ¹⁸O and δ³⁴S
values cover a wide range from 7.5 to 16.7 ‰ ± 0.5 ‰ (2σ) and from -2.66 to 13.99 ‰ ± 0.20 ‰ (2σ) with a

mean of 11.3 ± 2.4 ‰ and 3.78 ± 4.79 ‰ respectively. All samples have positive $\Delta^{17}\text{O}$ values, ranging from 0.08 to 2.56 ± 0.05 ‰ (2σ) with an average value of 0.86 ‰. Furthermore, it is noteworthy that 67 % of black crusts samples have $\Delta^{17}\text{O} > 0.65$ ‰. The $\Delta^{33}\text{S}$ and $\Delta^{36}\text{S}$ are both negative and vary between -0.34 and 0.00 ± 0.01 ‰ and between -0.76 and -0.22 ± 0.20 ‰ (2σ) respectively. No obvious correlation exists between $\delta^{18}\text{O}$, $\Delta^{17}\text{O}$, $\delta^{34}\text{S}$, $\Delta^{33}\text{S}$ and the distance from coastline (Fig. S1).

205 5. Discussion

5.1. The $\delta^{34}\text{S}$ - $\delta^{18}\text{O}$ - $\Delta^{17}\text{O}$ systematic

Sulfate in black crusts may have multiple origins that could be either primary and/or secondary. We refer to primary sulfates here as sulfates that are not formed in the atmosphere from SO_2 -oxidation. They can originate from the host-rock itself where sulfur occurs both as sulfide such as pyrite that would be subsequently dissolved and oxidized as sulfate, and as carbonate-associated sulfates (CAS), which substitute for carbonate in the lattice. Sulfates in black crusts can also have been directly emitted into the atmosphere for instance by sea-spray, resulting in sea-salt sulfate aerosols, or as products of combustion by refineries, vehicle exhaust or biomass burning; these commonly correspond to “primary sulfates” in the literature. On the contrary secondary sulfates result from the oxidation of tropospheric S-bearing gases (mainly SO_2) and other compounds including Dimethyl sulfide (DMS, $(\text{CH}_3)_2\text{S}$) by various oxidants (O_3 , H_2O_2 , OH, O_2 -TMI, NO_2 , ...). As black crusts are mainly constituted of gypsum ($\text{CaSO}_4 \cdot 2\text{H}_2\text{O}$), coupled $\delta^{34}\text{S}$ - $\delta^{18}\text{O}$ variations can be used to trace natural vs anthropogenic sources of sulfates in black crusts. Constrains on the primary/secondary origins of sulfate aerosols can also be brought by $\Delta^{17}\text{O}$ -values. Indeed, large positive $\Delta^{17}\text{O}$ anomalies in sulfate aerosols are inherited from their atmospheric oxidants that were produced during O_3 -photochemically induced genesis. In theory, other mechanisms exist such as magnetic isotope effect (see section 5.2.2) but have not been recognized yet. Resulting from photochemical reactions, O_3 molecules possess O-MIF compositions with $\Delta^{17}\text{O} \sim 35$ ‰ (Janssen et al., 1999; Lyons, 2001; Mauersberger et al., 1999) with lower value in the troposphere ~ 26 ‰ (Vicars and Savarino, 2014). Every molecule inheriting oxygen atoms from O_3 will also have positive $\Delta^{17}\text{O}$ including H_2O_2 with an average $\Delta^{17}\text{O} \sim 1.3$ ‰ (Savarino and Thiemens, 1999). OH, which isotopically exchanges with water vapor, and O_2 -TMI have mass-dependent composition with $\Delta^{17}\text{O} \sim 0$ (Dubey et al., 1997; Holt et al., 1981; Lyons, 2001) and ~ -0.34 ‰ (Barkan and Luz, 2005) respectively. Savarino (2000) measured the O-isotopic compositions of sulfates derived from these oxidation pathways and showed that OH and O_2 -TMI oxidation channels do not result in mass-independent fractionation signatures ($\Delta^{17}\text{O} = 0$ and -0.09 ‰ respectively) whereas O_3 and H_2O_2 radicals transfer $\frac{1}{4}$ and $\frac{1}{2}$ respectively of their isotopic anomaly to the sulfate thus resulting in mass-independent fractionation signatures ($\Delta^{17}\text{O} = 8.75$ ‰ and 0.65 ‰ respectively) (e.g. Bao et al., 2001a; Bao et al., 2000; Bao et al., 2001b; Bao et al., 2010; Jenkins and Bao, 2006; Lee et al., 2002; Lee and Thiemens, 2001; Li et al., 2013; Martin et al., 2014). Mass-dependent isotopic fractionation during SO_2 oxidation may change $\delta^{17}\text{O}$ and $\delta^{18}\text{O}$ but not the $\Delta^{17}\text{O}$ that only depends on the mixing of O-reservoirs with variable $\Delta^{17}\text{O}$. The fact that most black crusts have $\Delta^{17}\text{O} > 0.6$ ‰ demonstrates that a significant amount of sulfates is of atmospheric origin.

Black crusts sulfates analyzed in this study have O and S isotopic compositions that overlap other black crusts from Europe (Fig. 4; Longinelli & Bartelloni, 1978; Torfs et al., 1997, Kramar et al., 2011, Vallet et al., 2006)

and sulfate aerosols from USA and China (Fig. 5; Bao et al., 2001a; Jenkins and Bao, 2006; Lee and Thiemens, 2001; Li et al., 2013; Romero and Thiemens, 2003). In particular, there is a positive correlation between $\delta^{34}\text{S}$ and $\delta^{18}\text{O}$ covering a large range of variation of ~ 17 and ~ 9 ‰ respectively (Fig. 4), which can be interpreted in two ways: either a process leads to a variable enrichment or depletion of ^{18}O and ^{34}S in the crusts and/or it reflects a mixing between at least one depleted (in both ^{18}O and ^{34}S) and one enriched end-member. In the following paragraphs, we discuss in details the respective roles of several processes (e.g. partial SO_2 oxidation, mixing) that could lead to this correlation and overprint (or not) the source signatures. As previous studies, we will conclude that $\delta^{34}\text{S}$ - $\delta^{18}\text{O}$ - $\Delta^{17}\text{O}$ do record a mixing between different (natural and anthropogenic) sources, but addressing the role of processes is important (a pre-requisite) to assess the consistency of the $\Delta^{33}\text{S}$ anomaly origin.

5.1.1. Processes affecting O and S isotopic compositions

Firstly, gypsum precipitation would fractionate both O and S isotopes following a slope of 0.67 ± 0.02 (Fig. 4) when considering fractionation factors for $^{18}\text{O}/^{16}\text{O}$ between the dissolved sulfate and the gypsum ~ 1.002 or 1.0036 (experimental and natural values respectively) (Lloyd, 1968) and for $^{34}\text{S}/^{32}\text{S}$ ranges between 1.000 and 1.0024 (Ault and Kulp, 1959; Nielsen, 1974; Raab and Spiro, 1991; Thode et al., 1961) and a Rayleigh-type process in which black crusts represent the cumulated (precipitated) product at different residual fraction F of dissolved sulfates that are leached. However, the slope defined by the samples is steeper, ~ 1.52 ($R^2 = 0.58$) implying that the gypsum precipitation is not the main mechanism driving $\delta^{34}\text{S}$ and $\delta^{18}\text{O}$ variations in black crusts. Another process that could affect $\delta^{34}\text{S}$ - $\delta^{18}\text{O}$ -values is the partial oxidation of SO_2 by different oxidants (e.g. O_2 -TMI, H_2O_2 , O_3 , OH). Using the fractionation factors $^{34}\alpha_{\text{SO}_4\text{-SO}_2}$ obtained experimentally at 19°C by Harris et al. (2012a) for each oxidant ($^{34}\alpha_{\text{SO}_4\text{-SO}_2}(\text{OH}) = 1.0113 \pm 0.0024$; $^{34}\alpha_{\text{SO}_4\text{-SO}_2}(\text{H}_2\text{O}_2) = 1.0151 \pm 0.0013$; $^{34}\alpha_{\text{SO}_4\text{-SO}_2}(\text{O}_2\text{-TMI}) = 0.9894 \pm 0.0043$; $^{34}\alpha_{\text{SO}_4\text{-SO}_2}(\text{O}_3) = 1.0174 \pm 0.0028$) and their respective proportions from Sofen et al. (2011), usually cited in the literature for present day atmosphere (27 % OH ; 18 % $\text{O}_2\text{-TMI}$; 50 % H_2O_2 ; 5 % O_3), we calculated a global fractionation factor of 1.0097 . It is worth noting that these values produce a $\Delta^{17}\text{O}$ of 0.66 ‰ in agreement with our mean $\Delta^{17}\text{O}$ in black crusts. Consequently, following a Rayleigh distillation model and an initial SO_2 with $\delta^{34}\text{S} = 0$ ‰, the cumulated sulfates representing the black crusts would increase up to ~ 9 ‰ at maximum when < 10 % SO_2 is oxidized, which cannot explain the ~ 17 ‰ $\delta^{34}\text{S}$ -variation, especially since 40 % oxidized SO_2 is reported (Chin et al., 2000). To generate $\delta^{34}\text{S}$ -values as high as 17 ‰, O_3 and H_2O_2 oxidation pathways should increase drastically (i.e. requiring the absence of $\text{O}_2\text{-TMI}$ pathway), predicting an increase of $\Delta^{17}\text{O}$ up to ~ 6.5 ‰, which is not consistent with $\Delta^{17}\text{O} \sim 0$ ‰ associated with high $\delta^{34}\text{S}$ (Fig. 5). Therefore, SO_2 partial oxidation can explain a part of the data but not the whole isotope variations. The large $\delta^{34}\text{S}$ range could also reflect temporal variation, since in Greenland ice cores $\delta^{34}\text{S}$ was > 10 ‰ before the Industrial period (Patris et al., 2002), dominated by SO_2 from DMS (Sofen et al., 2011) and then decreased < 4 ‰ in the 1960's, dominated by anthropogenic SO_2 . Following this variation, black crusts on churches recently renovated should display low $\delta^{34}\text{S}$ and those renovated before the Industrial period should display higher $\delta^{34}\text{S}$. However, samples ME77-2 ($\delta^{34}\text{S} = -0.54$ ‰) and EV27-1 ($\delta^{34}\text{S} = 6.60$ ‰) compared to PY89-1 ($\delta^{34}\text{S} = 0.46$ ‰) gathered on churches restored after World War II and in 1772 respectively, present no significant temporal variation, that might be due to higher proportions of anthropogenic SO_2 emitted since recently (0.5 Tg S.yr^{-1} before Industrial

period and up to 69 Tg S.yr⁻¹ at present day; Sofen et al. (2011) and references therein). Thus, black crusts do not seem to record temporal isotopic variation, even if samples with $\delta^{34}\text{S} = -2.66$ and $\delta^{34}\text{S} = 13.99$ ‰ should be dated to confirm this assumption. Alternatively, with well-exposed surfaces to precipitation emphasizing wash-out and subsequent reprecipitation, black crusts could rather probe “recent” SO₂-oxidation. So far, no known processes
280 seem to affect the isotopic compositions, which rather probe the source signatures.

5.1.2 Source effects

If $\delta^{34}\text{S}$ - $\delta^{18}\text{O}$ variation reflects mixing of sources, at least two end-members are required. Determined graphically on Fig. 4 and 5, a first one would be ¹⁸O-³⁴S-enriched both around 18 ‰ with a near-zero $\Delta^{17}\text{O}$, which in view of
285 the sampling cross-section from NW to SE and west-dominating winds could correspond to the sea-sprays isotopic signature but available data usually display $\delta^{18}\text{O} \sim 9$ ‰ (Markovic et al., 2016) and $\delta^{34}\text{S} \sim 21$ ‰ (Rees et al., 1978), ruling out sea-sprays occurrence. The DMS produced by phytoplankton and oxidized in the atmosphere (11-25 TgS.yr⁻¹ being higher than sea-salt emissions (6-12 TgS.yr⁻¹ (Alexander et al., 2005) and references therein)), with $\delta^{34}\text{S}$ of 15-20 ‰ (Calhoun et al., 1991), sulfate aerosols deriving from DMS oxidation
290 could rather represent this ¹⁸O-³⁴S-enriched end-member. However, the absence of correlation between $\delta^{34}\text{S}$, $\delta^{18}\text{O}$, $\Delta^{17}\text{O}$ and the distance from coastline (Fig. S1) and near-zero $\Delta^{17}\text{O}$ for high $\delta^{34}\text{S}$ -values (Fig. 5) are not consistent with significant DMS contribution, mostly oxidized by O₃ (see above; Alexander et al., 2012). Despite some isolated halite crystals observed in one sample (Fig. 3e), we conclude that, overall, marine aerosols (DMS, sea-salt sulfates) do not relate to the high $\delta^{34}\text{S}$ - $\delta^{18}\text{O}$ -end-member. Major element contents (e.g. Na, Cl) have not
295 been measured here even if they could further constrain and quantify the presence of marine aerosols. The structural analyses of black crusts emphasize dissolution of the underlying carbonate. Carbonate-associated sulfates (with S abundances varying between a few tens to thousand ppm (Kampschulte and Strauss (2004) and references therein)) would also be dissolved and reprecipitated in black crusts and may well represent the enriched $\delta^{34}\text{S}$ - $\delta^{18}\text{O}$ end-member with near-zero $\Delta^{17}\text{O}$. CAS analyses from Atlantic and Pacific oceans over the
300 last 25 Myr and in the middle Cretaceous Tethys ocean show $\delta^{34}\text{S}$ from 11 to 24 ‰ with $\delta^{18}\text{O}$ from 5 to 21 ‰ similar to barite isotopic composition (Rennie and Turchyn, 2014; Turchyn et al., 2009). Furthermore, marine sulfates have typically $\Delta^{17}\text{O} \sim 0$ and > -0.2 ‰ in the geological record (Bao et al., 2008). CAS would thus perfectly match this end-member. Plaster used to seal blocks of carbonate stones are made through Lutetian gypsum dehydration and could also well represent the ¹⁸O-³⁴S-rich end-member. Indeed, Kloppmann et al. (2011)
305 measured $\delta^{34}\text{S}$ between 12.6 and 18.3 ‰ and $\delta^{18}\text{O}$ from 14.6 to 21.5 ‰ for mortars and plasters from French churches and castle. Thus, the surrounding plaster also matches this end-member, named CAS/PI on Fig. 4 and 5. The depleted end-member is graphically characterized by $\delta^{34}\text{S} < -3$ ‰ with little constrained $\delta^{18}\text{O}$, from 5 to 15 ‰ (Fig. 4, dashed box An) and $\Delta^{17}\text{O}$ from ~ 0 to 2.6 ‰ (Fig. 5, dashed box An). Sulfates from dissolved and oxidized sedimentary pyrites contained in the building carbonate stone are known to have $\delta^{34}\text{S} < -12$ ‰ (since at
310 least the last 500 Myr; Canfield, 2004). Despite a sulfide content that can vary between a few tens to a thousand ppm (Thomazo et al., 2018), our sampled carbonate stones are very whitish, suggesting a low sulfide content. Even if it would certainly not affect the mass balance, we took into account pyrite oxidation, as other studies did on black crusts (Kramar et al., 2011; Vallet et al., 2006). The S isotope fractionation factor during pyrite

oxidation being negligible (between 0.996 and 1; Thurston et al. (2010) and references therein) compared to O
315 isotopes, we modeled the $\delta^{18}\text{O}$ variation according to a Rayleigh distillation to represent the sulfide oxidation,
commonly occurring via $\text{O}_2 + \text{H}_2\text{O}$, at the atmosphere-carbonate building stone interface. With an initial $\delta^{18}\text{O} \sim -$
6 ‰ of rainwater in Paris Basin and a mean $^{18}\alpha_{\text{water-sulfate}}$ of 1.010 (Gomes and Johnston, 2017), sulfates from
pyrite oxidation would have $\delta^{18}\text{O} \sim 4$ ‰ and as low as -6 ‰ if water would be in limited amounts (i.e. residual
fraction of water $F \sim 0$). Very recently, pyrite oxidation was hypothesized to occur via O_3 (Hemingway et al.,
320 2019), which would lead to positive $\Delta^{17}\text{O}$ of sulfates with low $\delta^{34}\text{S}$, explaining the depleted end-member.
However, our data are strikingly higher than for black crusts from Ljubljana (Slovenia; (Kramar et al., 2011)),
which show $\delta^{34}\text{S}$ as low as -20 ‰ and $\delta^{18}\text{O}$ between -2 and 5 ‰ (Fig. 4) that would be typical for pyrite
oxidation. Besides, there is so far no evidence for a higher oxidation flux of pyrite via O_3 than major constituents
as H_2O and O_2 . This means that another source should have negative $\delta^{34}\text{S}$. Anthropogenic sulfur represent ~ 60 %
325 of the total sulfur released worldwide and includes primary sulfates as oil, coal and biomass combustion products
as well as SO_2 emission that can be oxidized into secondary sulfates. When considering coal and oil combustion,
 $\delta^{34}\text{S}$ can vary largely between -30 and 32 ‰ (e.g. Faure (1986)). More locally, a recent study reported a narrow
range between -0.57 and 11.33 ‰ for sulfur emitted by transport and industries in Paris (Au Yang et al., *in prep.*).
Lee et al., (2002) carried out herbs and diesel combustions resulting in $\delta^{34}\text{S}$ and $\delta^{18}\text{O}$ values between 9.55 and
330 16.42 ‰, and between 5.5 and 10.5 ‰ respectively with $\Delta^{17}\text{O} \sim 0$ ‰, forming primary sulfates without mass-
independent signatures. Because sulfate aerosols can be either primary or secondary with various SO_2 oxidation
pathways having distinct $\delta^{18}\text{O}$ - $\Delta^{17}\text{O}$ -values and O-fractionation factors, atmospheric aerosols would result in
variable $\delta^{18}\text{O}$ - $\Delta^{17}\text{O}$ -values. Therefore, the depleted end-member with $\delta^{34}\text{S} < -3$ ‰ and $0 < \Delta^{17}\text{O} < 0.65$ ‰ could
be typified by primary anthropogenic sulfate aerosols and/or SO_2 oxidized by OH or O_2 -TMI and/or a subtle
335 mixing of oxidation pathways to yield near-zero $\Delta^{17}\text{O}$ whereas samples with $\Delta^{17}\text{O} > 0.65$ ‰ rather point to a
significant anthropogenic SO_2 fraction oxidized by O_3 and H_2O_2 or by O_3 and to a lesser extent by O_2 -TMI and
OH, depending on the water pH (Lee and Thiemens, 2001) corresponding to secondary sulfate aerosols (named
An on Fig. 4 and Fig. 5). As the distinction between primary/secondary sulfate aerosols having near-zero $\Delta^{17}\text{O}$ is
not possible, we assume a mixing with only two end-members, CAS/Plaster and Anthropogenic sulfur (primary
340 and secondary). Furthermore, in view of the O isotope variability caused by the oxidation, mixing proportions
were calculated based only on $\delta^{34}\text{S}$ -values. We chose the end-members graphically and in agreement with the
literature, i.e. a CAS/PL $\delta^{34}\text{S}$ -value of 18 ‰, in the range from 11 to 24 ‰ (Kloppmann et al., 2011; Rennie and
Turchyn, 2014; Turchyn et al., 2009)(Fig. 4) and an An $\delta^{34}\text{S}$ -value of -3 ‰, similar to Montana et al. (2008) as
well the closest to sulfates measured in Paris. CAS/PL proportions range between 2 and 81 % with an average \sim
345 32 %. With an extreme $\delta^{34}\text{S}$ of -10 ‰ for An end-member, encompassing black crusts from Antwerp, CAS/PL
proportion average at 49 %. This highlights that host rock sulfate is on average not the main S-provider and that
black crusts record atmospheric sulfate aerosols. Excluding the most “contaminated” samples by CAS/PL and
assuming that those having $\Delta^{17}\text{O} > 0.65$ ‰ obviously represent SO_2 oxidized by O_3 and H_2O_2 , the minimum
proportion of MIF-bearing sulfates, and hence secondary sulfates can be estimated ~ 63 % which is close to
350 estimations of Lee and Thiemens (2001) and Sofen et al. (2011). In summary, black crusts sample significant

amounts of atmospheric SO₂ and complement existing sampling such as aerosols, which allow us to address the origin of $\Delta^{33}\text{S}$ anomaly.

5.2. Black crusts S-MIF signature

355

5.2.1 Processes implicated in black crust formation

$\Delta^{33}\text{S}$ - $\Delta^{36}\text{S}$ -values recorded by black crust sulfates range between -0.34 and 0.00 ± 0.01 ‰ for $\Delta^{33}\text{S}$ and between -0.76 and -0.22 ± 0.20 ‰ (2σ) for $\Delta^{36}\text{S}$ (Table 2). These values are quite unusual compared with anthropogenic and natural aerosols. As illustrated by Fig. 6, black crust sulfates $\Delta^{33}\text{S}$ -values are all negative and it is worth noting that this depletion occurs with near constant $\Delta^{36}\text{S}$ -values. This is somewhat distinct from most aerosols, which display almost exclusively positive $\Delta^{33}\text{S}$ up to ~ 0.5 ‰ and both positive and negative $\Delta^{36}\text{S}$ (Au Yang et al., 2019; Guo et al., 2010; Lin et al., 2018b; Romero and Thiemens, 2003; Shaheen et al., 2014). So far the only negative $\Delta^{33}\text{S}$ -values down to -0.6 ‰ were measured in sulfate aerosols from Beijing (China) during one winter month (Han et al., 2017), (no $\Delta^{36}\text{S}$ -values provided) and these values were assumed to result from incomplete combustion of coal. This assumption ultimately relies on the work of Lee et al. (2002), which showed that primary anthropogenic aerosols formed by high temperature combustion (e.g. diesel) result in near-zero $\Delta^{33}\text{S}$ - $\Delta^{36}\text{S}$ -values whereas those formed by low temperature combustion (e.g. biomass burning) result in $\Delta^{33}\text{S}$ down to -0.2 ‰ and $\Delta^{36}\text{S}$ -values varying between -1.9 and 0.2 ‰ (data recalculated with $^{36}\beta = 1.9$). Negative $\Delta^{36}\text{S}$ -values well correlated with biomass burning proxies are also reported in East China (Lin et al., 2018b) although $\Delta^{33}\text{S} \sim 0$ ‰. As many other cities, Paris has long been affected by coal and wood burning, we can hypothesize that $\Delta^{33}\text{S}$ - $\Delta^{36}\text{S}$ variations result from high and/or low temperature combustion processes. Some black crust sulfates with near-zero $\Delta^{33}\text{S}$ - $\Delta^{36}\text{S}$ -values could result from high temperature combustion but this would not explain negative $\Delta^{33}\text{S}$ - $\Delta^{36}\text{S}$. Furthermore, according to Lin et al. (2018b), low temperature combustion would preferentially fractionate ^{36}S over ^{33}S , which should result in a steep slope in a $\Delta^{33}\text{S}$ - $\Delta^{36}\text{S}$ space. The trend defined by our black crust samples shows higher ^{33}S fractionation than ^{36}S with $\Delta^{33}\text{S}$ -values lower than that obtained by available low temperature combustion experiments (< -0.2 ‰; Lee et al., 2002) and with $\Delta^{36}\text{S}$ -values in the range of aerosols. Furthermore, no $\Delta^{33}\text{S}$ evolution is observed in black crusts sampled on churches with different ages of renovation (see section 5.1; ME77-2 $\Delta^{33}\text{S} = -0.21$ ‰; EV27-1 $\Delta^{33}\text{S} = -0.05$ ‰; and PY89-1 $\Delta^{33}\text{S} = -0.21$ ‰) whereas we would expect a $\Delta^{33}\text{S}$ -increase in black crusts from -0.2 ‰ and 0 ‰ due to the reduction of sulfur emission from low temperature replaced by high temperature combustion processes. Therefore, available data highlight that neither high nor low temperature combustion processes are responsible for low $\Delta^{33}\text{S}$ measured in black crusts. Part of black crust sulfates being atmospheric in origin, isotopic effects during SO₂ oxidation could be responsible for $\Delta^{33}\text{S}$ - $\Delta^{36}\text{S}$ variations. To better address this issue, we calculated the $\Delta^{33}\text{S}$ - $\Delta^{36}\text{S}$ -values of sulfates predicted by each of the main SO₂ oxidation pathways and by a mixing of them in the proportions given by Sofen et al. (2011). We used $^{33}\beta$ and $^{36}\beta$ determined by experiments of SO₂ oxidation by O₂-TMI, H₂O₂, O₃, OH (Harris et al. (2013b) and values cited in Au Yang et al. (2018); see caption text) and NO₂ (Au Yang et al., 2018) and T-dependent equations determined by Harris et al. (2013b) to calculate each $^{34}\alpha$ with initial sulfur dioxide $\Delta^{33}\text{S}$ and $\Delta^{36}\text{S}$ of 0 ‰ (Lin et al., 2018b). As mentioned earlier (Au Yang et al., 2018; Harris et al., 2013b), none of these models can account for anomalous $\Delta^{33}\text{S}$ - $\Delta^{36}\text{S}$ values in either aerosols or in black crusts (Fig. 6). Although

385

390 oxidation with O₂-TMI at T = 50°C could produce negative Δ³³S down to -0.37‰ which would account for the
lowest Δ³³S observed in black crust, this oxidation pathway would also produce larger Δ³⁶S down to -1.50 ‰ at
odds with the Δ³⁶S reported in the black crust. Their potential combination cannot account for sulfate aerosols
data from the literature (Au Yang et al., 2019; Guo et al., 2010; Lin et al., 2018b; Romero and Thiemens, 2003;
Shaheen et al., 2014), neither for the black crust as it would result in slightly negative Δ³³S-Δ³⁶S that could not
395 explain the Δ³³S as low as -0.34 ‰ (yellow frames on Fig. 6). Available literature data are therefore not
consistent with the anomalous Δ³³S-Δ³⁶S-values recorded in black crust sulfates.

Mass-dependent processes can also result in small Δ³³S-Δ³⁶S variations, depending on the magnitude of the ³⁴S
fractionation (Ono et al., 2006a). As mentioned in section 5.1.2, a mixing between a ^{33,34}S depleted end-member
(An) consisting of anthropogenic sulfur (δ³⁴S = -3 ‰, Δ³³S = 0 ‰) and a ^{33,34}S enriched sulfates end-member
400 (CAS/PL) from plaster or CAS (δ³⁴S = 18 ‰, Δ³³S = 0 ‰) would result in small Δ³³S of -0.01 ‰ for 50 %
mixing, which is far from the maximum measured Δ³³S ~ -0.34. Moreover, the slope between Δ³³S-Δ³⁶S would be
about -7 at odd with our observations. Therefore, we conclude that mixing cannot account for the black crusts
Δ³³S-Δ³⁶S variations.

405 5.2.2 A new oxidation pathway implying magnetic isotope effect

Several studies proposed that positive Δ³³S measured in sulfate aerosols, with Δ³³S up to 0.5 ‰, from e.g. East
China and California could result from stratospheric fallout of SO₂ (with Δ³³S potentially up to 10 ‰ higher; Ono
et al. (2013)), which underwent UV photolysis by short wavelength (Romero and Thiemens, 2003; Lin et al.,
2018a; Lin et al., 2018b). This suggestion primarily relies on the similarities between Δ³³S-Δ³⁶S values of sulfate
410 aerosols and laboratory experiments of SO₂ photolysis conducted at different wavelengths (Romero and
Thiemens, 2003) and on the correlation between ³⁵S specific activity and Δ³³S-values (Lin et al., 2018b).
However, these studies never addressed the absence of the complementary negative Δ³³S-reservoir, which is
required to balance the positive Δ³³S-reservoir (see Au Yang et al., 2019). In this respect, it is worth mentioning
that volcanic and stratospheric aerosols trapped in Antarctic ice cores (see Gautier et al. (2018) and references
415 therein) show both positive Δ³³S (up to ~ 2 ‰) and complementary negative Δ³³S-values (down to -1 ‰) and
weighed average Δ³³S ≠ 0 ‰ explained by prior partial deposition. Stratospheric fluxes are actually too low to
account for Δ³³S > 0.1 ‰ (Lin et al., 2016; Au Yang et al., 2019). Accordingly, some other authors rather tried to
explain the positive anomalies of most aerosols with ‘tropospheric’ chemical reactions, that are SO₂ oxidation by
the main oxidant including NO₂, H₂O₂, OH, O₃ and O₂-TMI, but experimental data results in a maximum Δ³³S ~
420 0.2 ‰ for all studied reactions (Au Yang et al., 2018; Harris et al., 2013b). Isotope effects associated with SO₂-
oxidation by minor species, such as Criegee radicals remains to be investigated (Au Yang et al., 2018). In
summary, whatever the stratospheric vs. tropospheric origin of positive Δ³³S-values recorded by most aerosols,
there is a ³³S-isotope imbalance and a missing reservoir with negative Δ³³S that must exist. Han et al. (2017)
reported Δ³³S-values down to -0.6 ‰ in sulfate aerosols from Beijing. As discussed above, the authors’
425 suggestion calling for low temperature combustion is little supported by available data, and clearly the very
restricted location and time interval, over a month, where these anomalies occurred cannot counter balance, both
spatially and temporally, the common positive Δ³³S-values of most aerosols; the missing reaction/reservoir
requires, instead, to be ubiquitous worldwide.

In this study, black crust sulfates display negative $\Delta^{33}\text{S}$ -values (from ~ 0 ‰ down to -0.34 ‰). These values are
430 certainly produced by tropospheric chemical reactions. They would otherwise, according to the stratospheric
origin model, have the same sign as those measured among aerosols. Furthermore, the(se) chemical reaction(s)
involved in the formation of black crusts must be distinct than those leading to the formation of tropospheric
aerosols. As developed thoroughly, black crust could well represent the missing sulfur reservoir.

An additional observation is that negative $\Delta^{33}\text{S}$ -values occur with near constant $\Delta^{36}\text{S}$ (from -0.76 to -0.22 ± 0.20
435 ‰; Fig. 6). This signature is typical of magnetic isotope effects (MIE), which involve a radical pair, where
coupling between the nuclear magnetic moment of the nucleus of odd isotopes and the electron occurs, allowing
for electron spin transition from singlet to triplet (or vice-versa) (Buchachenko et al., 1976). This leads to distinct
half-lives between odd and even isotopes resulting in specific odd over even isotope enrichment (or depletion).
MIE has been so far reported for various reactions occurring on a surface (Buchachenko, 2001, 2000; Turro,
440 1983) like sulfate thermochemical reduction (Oduro et al., 2011) or Fe reduction in magneto-tactic bacteria
(Amor et al., 2016) for the most geologically relevant. It is worth pointing out that MIE could also be responsible
for positive $\Delta^{17}\text{O}$ measured in black crusts, i.e. as opposed to $\Delta^{17}\text{O}$ -anomaly being inherited from SO_2 oxidants.
However, Lee et al. (2002) also measured the O-multi isotopic compositions of sulfate aerosols (i.e. from the
atmosphere as opposed to reaction on a solid substrate) from Paris and obtained $\Delta^{17}\text{O} = 0.2$ and 0.8 ‰ for the
445 Paris highway and in the 13th zone respectively, which is in good agreement with our three samples collected in
Paris (from 0.17 to 0.89 ‰). Thus, this is consistent with black crust formation recording mostly an atmospheric
signal and no significant magnetic isotope effect on $\Delta^{17}\text{O}$.

Magnetic effect could occur on a surface such as on mineral dust suspended in the atmosphere, during aerosols
450 formation, leading to residual ^{33}S -depleted atmospheric SO_2 from which black crusts would subsequently formed.
This model would however predict some sulfate aerosols formed subsequently to display negative $\Delta^{33}\text{S}$: such
values are extremely uncommon being primarily restricted to the Beijing winter month (Han et al., 2017).
Instead, magnetic effect could occur during black crust formation, on the carbonate building stone, leading to
residual ^{33}S -enriched atmospheric SO_2 from which tropospheric aerosols would subsequently formed; which is
455 consistent with available observations. This model would however predict some black crust formed subsequently
to display positive $\Delta^{33}\text{S}$: such values have not been found yet and this may well reflect sample bias, our data
being the first reported for such samples. Both scenario imply non-zero $\Delta^{33}\text{S}$ of residual atmospheric SO_2 which
contrast with the data by Lin et al. (2018b) showing $\Delta^{33}\text{S} \sim 0$ ‰ ($n = 5$, $\Delta^{33}\text{S}$ varying from -0.04 to 0.01 ± 0.01
‰). Given that, in the study of Lin et al. (2018b), SO_2 was sampled close to the third largest Chinese megacity,
460 such non-zero $\Delta^{33}\text{S}$ -values may thus be rather symptomatic of emitted (i.e. anthropogenic) SO_2 rather than
residual/background (i.e. after significant black crust and aerosols formation). SO_2 in the Paris basin still has to
be measured to confirm this assumption but so far, this could be consistent with the interpretation that non-zero
 $\Delta^{33}\text{S}$ -values of residual/background atmospheric SO_2 are erased by anthropogenic SO_2 having zero $\Delta^{33}\text{S}$ -values
(Au Yang et al., 2019) moving towards the local source(s) of anthropogenic SO_2 .

In the absence of additional observations, proposing a chemical reaction, and hence a radical pair that breaks and
465 recombines, would be very speculative, but our data clearly point towards the occurrence of magnetic effect
occurring during the formation of black crust, involving ubiquitous heterogeneous chemical reactions. This is

supported by previous recognition of sulfur radicals such as SO_x^- (Herrmann, 2003) or S-S (see Babikov (2017) but note that their $\Delta^{36}\text{S}/\Delta^{33}\text{S}$ slope is distinct from ours). Clearly, the reaction does not occur after sulfate
470 formation such as during dissolution/precipitation mechanisms, which does not involve any radical species. As mentioned above, magneto-tactic bacteria can produce MIE when reducing Fe (Amor et al., 2016). Microbial activity being sometimes present on black crusts (Gaylarde et al., 2007; Sáiz-Jiménez, 1995; Scheerer et al., 2009; Schiavon, 2002; Tiano, 2002), the involvement of micro-organisms, affecting only the sulfur isotopes as the most negative $\Delta^{33}\text{S}$ does not correspond to the most negative $\Delta^{17}\text{O}$, represents another possibility to
475 investigate. Another implication that can be tested in future work is that the kinetics of heterogeneous reactions leading to sulfate and black crust formation should be comparable or faster than those leading to aerosol formation. So far, Li et al. (2006) showed comparable loss of atmospheric SO_2 by heterogeneous oxidation on calcium carbonate substrate and by gas phase oxidation. Our conclusions show strong analogy with the model of Au Yang et al. (2019) who suggest SO_2 photo-oxidation on mineral dust could form sulfate aerosols depleted in
480 ^{33}S that would then be deposited. The residual SO_2 would be subsequently enriched in ^{33}S , then be oxidized by common O_3 , H_2O_2 , O_2 , OH oxidants. Their ^{33}S -depletion mechanism was not further constrained, except that it was speculated to be photochemical in origin.

If correct, this view requires reassessing the overall S-isotope fractionation during SO_2 atmospheric reaction. So far, previous studies assumed that the overall sulfur isotopic fractionation between the wet/dry deposit and
485 oxidized SO_2 was equal to 1 (i.e. no isotope effect), but negative $\Delta^{33}\text{S}$ in black crusts is inconsistent with such an assumption.

Starting with SO_2 $\Delta^{33}\text{S}$ -value of 0 ‰ (Au Yang et al., 2018; Lin et al., 2018b) and forming oxidized (sampled by secondary aerosols) and wet/dry deposit (sampled by black crusts) reservoirs with $\Delta^{33}\text{S}$ -values up to 0.50 ‰ down to -0.34 ‰ respectively, mass balance imposes that SO_2 dry/wet depositions and secondary sulfate aerosols
490 represents ~60 and 40 % respectively. This is in good agreement with proportions obtained by Chin et al. (2000) and quoted by Harris et al. (2013b). Therefore, we conclude that MIE happening during SO_2 dry and wet depositions could be a viable mechanism responsible for ^{33}S -enrichment of secondary sulfate aerosols and that black crusts could represent the ^{33}S -negative complementary reservoir.

In order to better apprehend the aerosols/black crust complementarity, we modeled the S-isotopic fractionation of
495 both black crusts and aerosols during SO_2 oxidation (Fig. 6 and 7). We assumed a Rayleigh distillation model to represent the atmosphere-building stone interface open system. The global fractionation factor between residual SO_2 and oxidized (secondary aerosols) + deposited (black crusts) SO_2 is defined as $\alpha_{\text{global}} = A \alpha_{\text{BC-SO}_2} \times B \alpha_{\text{aerosols-SO}_2}$ with A and B the proportions of SO_2 deposited and oxidized, being equal to 60 and 40 % respectively. This allows us to deduce the $^{33, 34, 36}\alpha_{\text{BC-SO}_2}$ and the associated $^{33, 36}\beta$ factor. A $\delta^{34}\text{S}$ of 1 ‰ for the initial SO_2 was
500 considered to obtain black crusts of at least -3 ‰ (see section 5.1.2) and $\Delta^{33}\text{S}-\Delta^{36}\text{S} = 0$ ‰; $^{34}\alpha_{\text{aerosols-SO}_2}$ was taken as 1.0097 as calculated using the different oxidation channels proportions of Sofen et al. (2011). The oxidation being mass-dependent, we chose $^{33, 36}\beta_{\text{aerosols-SO}_2}$ of 0.515 and 1.9 respectively (Harris et al., 2012). The best fit is obtained for $^{34}\alpha_{\text{BC-SO}_2} = 0.9985$, $^{33}\alpha_{\text{BC-SO}_2} = 0.9986$ and $^{36}\alpha_{\text{BC-SO}_2} = 0.9972$ with $^{33, 36}\beta = 0.9$ and 1.9 respectively. The ^{33}S -enrichment in secondary sulfate aerosols is well represented by this parameterization (instantaneous and
505 cumulated products; Fig. 6 and 7). The concomitant ^{33}S -depletion in modeled cumulated deposit is also well represented. The ^{33}S -isotopic fractionation occurring during the MIE is higher than the one observed in black

crusts. At first order this model works, predicting the total cumulated products of black crusts and aerosols to have $\Delta^{33}\text{S}$ -values of -0.23 and 0.35 ‰ respectively. The match is not perfect, capturing not entirely black crusts isotopic compositions, but remember that black crusts are produced from anthropogenic Parisian SO_2 whereas aerosols formed in other locations possibly formed from distinct anthropogenic SO_2 $\delta^{34}\text{S}$ -values. In addition, we are aware that our model strongly depends on oxidation pathways estimated by Sofen et al. (2011), which vary spatially and temporally. The main weakness is the too little constrained estimate of intrinsic S-bearing compounds (CAS/plaster end-member) in the host-rock as well as sulfate aerosols ($\Delta^{33}\text{S} > 0$ ‰) which dilutes the ^{33}S anomaly, lowering the overall black crust $\Delta^{33}\text{S}$. Ultimately, black crusts result mainly from the deposition followed by oxidation of SO_2 on the building stone rather than aerosols accumulation. The $\delta^{34}\text{S}$ -value of initial anthropogenic SO_2 is another poorly constrained parameter whose variability might be difficult to estimate both spatially and temporally.

In conclusion, black crusts could represent the complementary sulfur end-member to sulfate aerosols. Its fractionation factor is relatively restricted (-1.5 ‰) and is thus likely identifiable from its negative $\Delta^{33}\text{S}$ -values. Our model is actually consistent with assumption that the global SO_2 oxidation occurs with little fractionation ($^{34}\alpha_{\text{global}} = 1.00298$) as commonly done in the literature. Finally, figure 8 summarizes the different sulfur sources involved in the black crusts as well as the processes leading to their formation. Black crusts isotopic compositions could thus be explained by a mixing between sulfates from CAS/plaster ($\delta^{34}\text{S} \sim 18$ ‰ and $\Delta^{33}\text{S} = 0$ ‰, see section 5.1 and 1 on Fig. 8), primary anthropogenic sulfates ($\delta^{34}\text{S} \sim -3$ ‰ and $\Delta^{33}\text{S} = 0$ ‰; see 2 on Fig. 8) and wet/dry deposition of SO_2 undergoing MIE during its oxidation on the building stone combined with secondary aerosols (see red triangle on Fig. 7 and 3 on Fig. 8).

6. Conclusion

Our study shows that black crusts do preserve an atmospheric signal of SO_2 oxidation, inferred from the non-zero $\Delta^{17}\text{O}$. Part of the sulfate originates from the surrounding plaster and/or from the stone itself but overall > 60 % originate from anthropogenic activities. We also discovered negative $\Delta^{33}\text{S}$ with near constant $\Delta^{36}\text{S}$ signatures, which probably reflect magnetic isotope effect involving a new oxidation pathway. Magnetic isotope effect is supposed to occur during the deposit of SO_2 on building stone surface (most likely carbonate), where SO_2 is oxidized into sulfate leading to a ^{33}S -depletion in black crust sulfates. Therefore, the resulting ^{33}S -enrichment of residual SO_2 could account for positive $\Delta^{33}\text{S}$ -values of sulfate aerosols observed worldwide, making black crust sulfates their complementary $\Delta^{33}\text{S}$ reservoir.

Data availability

All data needed to draw the conclusions in the present study are shown in this paper and/or the Supplement. For additional data related to this study, please contact the corresponding author (genot@ipgp.fr).

Author contributions

IG conducted oxygen isotope measurements under the supervision of EM and ELG at IPGP. DAY conducted
545 sulfur isotope measurements at McGill University. IG and EM collected the samples. IG, PC, EM and DAY
interpreted the data. IG wrote the paper with contributions from all coauthors. EM and MR conceived the project.

Acknowledgments

This project was supported by a grant from the Agence Nationale de la Recherche (ANR) via contract 14-CE33-
550 0009-02-FOFAMIFS. We thank the editor Eliza Harris, Mang Lin and an anonymous reviewer for their insightful
comments as well as Mark Thiemens for his remarks on MIE that helped improving our manuscript. We thank
David Whiteley and Rémi Leprêtre for their help during the sampling, Mattauer for inspiration, Omar Boudouma
for the SEM analysis, Boswell Wing for accessing his laboratory and Hao Thi Bui for assistance during analyses
performed in Montreal, Nelly Assayag and Guillaume Landais for those performed at IPGP.

555

Competing interests

The authors declare that they have no conflict of interest.

References

- 560 Alexander, B., Allman, D., Amos, H., Fairlie, T., Dachs, J., Hegg, D. A., and Sletten, R. S.: Isotopic constraints
on the formation pathways of sulfate aerosol in the marine boundary layer of the subtropical northeast Atlantic
Ocean, *Journal of Geophysical Research: Atmospheres*, 117, 2012.
Alexander, B., Park, R. J., Jacob, D. J., Li, Q., Yantosca, R. M., Savarino, J., Lee, C., and Thiemens, M.: Sulfate
formation in sea-salt aerosols: Constraints from oxygen isotopes, *Journal of Geophysical Research: Atmospheres*,
565 110, 2005.
Amor, M., Busigny, V., Louvat, P., Gélabert, A., Cartigny, P., Durand-Dubief, M., Ona-Nguema, G.,
Alphandéry, E., Chebbi, I., and Guyot, F.: Mass-dependent and-independent signature of Fe isotopes in
magnetotactic bacteria, *Science*, 352, 705-708, 2016.
Ault, W. U. and Kulp, J.: Isotopic geochemistry of sulphur, *Geochimica et Cosmochimica Acta*, 16, 201-235,
570 1959.
Au Yang, D., Bardoux, G., Assayag, N., Laskar, C., Widory, D., and Cartigny, P.: Atmospheric SO₂ oxidation by
NO₂ plays no role in the mass independent sulfur isotope fractionation of urban aerosols, *Atmospheric
Environment*, 193, 109-117, 2018.
Au Yang, D., Cartigny, P., Desboeufs, K., and Widory, D.: Seasonality in the $\Delta^{33}\text{S}$ measured in urban aerosols
575 highlights an additional oxidation pathway for atmospheric SO₂, *Atmospheric Chemistry and Physics*, 19, 3779-
3796, 2019.
Au Yang, D., Landais, G., Assayag, N., Widory, D., and Cartigny, P.: Improved analysis of micro-and nanomole-
scale sulfur multi-isotope compositions by gas source isotope ratio mass spectrometry, *Rapid Communications in
Mass Spectrometry*, 30, 897-907, 2016.
580 Babikov, D.: Recombination reactions as a possible mechanism of mass-independent fractionation of sulfur
isotopes in the Archean atmosphere of Earth, *Proceedings of the National Academy of Sciences*, 114, 3062-3067,
2017.
Bao, H.: Purifying barite for oxygen isotope measurement by dissolution and reprecipitation in a chelating
solution, *Analytical chemistry*, 78, 304-309, 2006.
585 Bao, H., Lyons, J., and Zhou, C.: Triple oxygen isotope evidence for elevated CO₂ levels after a Neoproterozoic
glaciation, *Nature*, 453, 504, 2008.
Bao, H., Michalski, G. M., and Thiemens, M. H.: Sulfate oxygen-17 anomalies in desert varnishes, *Geochimica
et Cosmochimica Acta*, 65, 2029-2036, 2001a.
Bao, H. and Thiemens, M. H.: Generation of O₂ from BaSO₄ Using a CO₂- Laser Fluorination System for
590 Simultaneous Analysis of $\delta^{18}\text{O}$ and $\delta^{17}\text{O}$, *Analytical chemistry*, 72, 4029-4032, 2000.
Bao, H., Thiemens, M. H., Farquhar, J., Campbell, D. A., Lee, C. C.-W., Heine, K., and Loope, D. B.:
Anomalous ¹⁷O compositions in massive sulphate deposits on the Earth, *Nature*, 406, 176, 2000.

- Bao, H., Thiemens, M. H., and Heine, K.: Oxygen-17 excesses of the Central Namib gypcretes: spatial distribution, *Earth and Planetary Science Letters*, 192, 125-135, 2001b.
- 595 Bao, H., Yu, S., and Tong, D. Q.: Massive volcanic SO₂ oxidation and sulphate aerosol deposition in Cenozoic North America, *Nature*, 465, 909, 2010.
- Barkan, E. and Luz, B.: High precision measurements of 17O/16O and 18O/16O ratios in H₂O, *Rapid Communications in Mass Spectrometry: An International Journal Devoted to the Rapid Dissemination of Up-to-the-Minute Research in Mass Spectrometry*, 19, 3737-3742, 2005.
- 600 Bigeleisen, J. and Mayer, M. G.: Calculation of equilibrium constants for isotopic exchange reactions, *The Journal of Chemical Physics*, 15, 261-267, 1947.
- Bindeman, I., Eiler, J., Wing, B., and Farquhar, J.: Rare sulfur and triple oxygen isotope geochemistry of volcanogenic sulfate aerosols, *Geochimica et Cosmochimica Acta*, 71, 2326-2343, 2007.
- Buchachenko, A., Galimov, E., Ershov, V., Nikiforov, G., and Pershin, A.: Isotopic enrichment induced by magnetic-interactions in chemical-reactions, *Doklady Akademii Nauk Sssr*, 228, 379-381, 1976.
- 605 Buchachenko, A. L.: Magnetic isotope effect: Nuclear spin control of chemical reactions, *The Journal of Physical Chemistry A*, 105, 9995-10011, 2001.
- Buchachenko, A. L.: Recent advances in spin chemistry, *Pure and applied chemistry*, 72, 2243-2258, 2000.
- Cabral, R. A., Jackson, M. G., Rose-Koga, E. F., Koga, K. T., Whitehouse, M. J., Antonelli, M. A., Farquhar, J., Day, J. M., and Hauri, E. H.: Anomalous sulphur isotopes in plume lavas reveal deep mantle storage of Archaean crust, *Nature*, 496, 490, 2013.
- 610 Calhoun, J. A., Bates, T. S., and Charlson, R. J.: Sulfur isotope measurements of submicrometer sulfate aerosol particles over the Pacific Ocean, *Geophysical Research Letters*, 18, 1877-1880, 1991.
- Camuffo, D.: Physical weathering of stones, *Science of the Total Environment*, 167, 1-14, 1995.
- 615 Canfield, D. E.: The evolution of the Earth surface sulfur reservoir, *American Journal of Science*, 304, 839-861, 2004.
- Chin, M., Rood, R. B., Lin, S. J., Müller, J. F., and Thompson, A. M.: Atmospheric sulfur cycle simulated in the global model GOCART: Model description and global properties, *Journal of Geophysical Research: Atmospheres*, 105, 24671-24687, 2000.
- 620 Cowie, B. R. and Johnston, D. T.: High-precision measurement and standard calibration of triple oxygen isotopic compositions ($\delta^{18}\text{O}$, $\Delta^{17}\text{O}$) of sulfate by F₂ laser fluorination, *Chemical Geology*, 440, 50-59, 2016.
- Dauphas, N. and Schauble, E. A.: Mass fractionation laws, mass-independent effects, and isotopic anomalies, *Annual Review of Earth and Planetary Sciences*, 44, 709-783, 2016.
- Defouilloy, C., Cartigny, P., Assayag, N., Moynier, F., and Barrat, J.-A.: High-precision sulfur isotope composition of enstatite meteorites and implications of the formation and evolution of their parent bodies, *Geochimica et Cosmochimica Acta*, 172, 393-409, 2016.
- 625 Delavault, H., Chauvel, C., Thomassot, E., Devey, C. W., and Dazas, B.: Sulfur and lead isotopic evidence of relic Archean sediments in the Pitcairn mantle plume, *Proceedings of the National Academy of Sciences*, 113, 12952-12956, 2016.
- 630 Dubey, M. K., Mohrschladt, R., Donahue, N. M., and Anderson, J. G.: Isotope specific kinetics of hydroxyl radical (OH) with water (H₂O): Testing models of reactivity and atmospheric fractionation, *The Journal of Physical Chemistry A*, 101, 1494-1500, 1997.
- Farquhar, J., Bao, H., and Thiemens, M.: Atmospheric influence of Earth's earliest sulfur cycle, *Science*, 289, 756-758, 2000.
- 635 Farquhar, J., Savarino, J., Airieau, S., and Thiemens, M. H.: Observation of wavelength-sensitive mass-independent sulfur isotope effects during SO₂ photolysis: Implications for the early atmosphere, *Journal of Geophysical Research: Planets*, 106, 32829-32839, 2001.
- Farquhar, J., Johnston, D. T., and Wing, B. A.: Implications of conservation of mass effects on mass-dependent isotope fractionations: influence of network structure on sulfur isotope phase space of dissimilatory sulfate reduction, *Geochimica et Cosmochimica Acta*, 71, 5862-5875, 2007a.
- 640 Farquhar, J., Peters, M., Johnston, D. T., Strauss, H., Masterson, A., Wiechert, U., and Kaufman, A. J.: Isotopic evidence for Mesoarchean anoxia and changing atmospheric sulphur chemistry, *Nature*, 449, 706, 2007b.
- Farquhar, J., Wing, B., McKeegan, K., Harris, J., Cartigny, P., and Thiemens, M.: Mass-independent sulfur of inclusions in diamond and sulfur recycling on early Earth, *Science*, 298, 2369-2372, 2002.
- 645 Farquhar, J. and Wing, B. A.: Multiple sulfur isotopes and the evolution of the atmosphere, *Earth and Planetary Science Letters*, 213, 1-13, 2003.
- Faure, G.: *Isotope systematics in two-component mixtures*, John Wiley and Sons, 1986.
- Forster, P., Ramaswamy, V., Artaxo, P., Bernsten, T., Betts, R., Fahey, D. W., Haywood, J., Lean, J., Lowe, D. C., and Myhre, G.: Changes in atmospheric constituents and in radiative forcing. Chapter 2. In: *Climate Change*
- 650 2007. The Physical Science Basis, 2007.

- Fronteau, G., Schneider-Thomachot, C., Chopin, E., Barbin, V., Mouze, D., and Pascal, A.: Black-crust growth and interaction with underlying limestone microfacies, Geological Society, London, Special Publications, 333, 25-34, 2010.
- 655 Gautier, E., Savarino, J., Erbland, J., and Farquhar, J.: SO₂ Oxidation Kinetics Leave a Consistent Isotopic Imprint on Volcanic Ice Core Sulfate, *Journal of Geophysical Research: Atmospheres*, 123, 9801-9812, 2018.
- Gaylarde, C. C., Ortega-Morales, B. O., and Bartolo-Perez, P.: Biogenic black crusts on buildings in unpolluted environments, *Curr Microbiol*, 54, 162-166, 2007.
- Gomes, M. L. and Johnston, D. T.: Oxygen and sulfur isotopes in sulfate in modern euxinic systems with implications for evaluating the extent of euxinia in ancient oceans, *Geochimica et Cosmochimica Acta*, 205, 331-359, 2017.
- 660 Guo, Z., Li, Z., Farquhar, J., Kaufman, A. J., Wu, N., Li, C., Dickerson, R. R., and Wang, P.: Identification of sources and formation processes of atmospheric sulfate by sulfur isotope and scanning electron microscope measurements, *Journal of Geophysical Research: Atmospheres*, 115, 2010.
- 665 Han, X., Guo, Q., Strauss, H., Liu, C., Hu, J., Guo, Z., Wei, R., Peters, M., Tian, L., and Kong, J.: Multiple sulfur isotope constraints on sources and formation processes of sulfate in Beijing PM_{2.5} aerosol, *Environmental science & technology*, 51, 7794-7803, 2017.
- Harris, E., Sinha, B., Foley, S., Crowley, J., Borrmann, S., and Hoppe, P.: Sulfur isotope fractionation during heterogeneous oxidation of SO₂ on mineral dust, *Atmospheric Chemistry and Physics*, 12, 4867-4884, 2012a.
- 670 Harris, E., Sinha, B., Hoppe, P., Crowley, J., Ono, S., and Foley, S.: Sulfur isotope fractionation during oxidation of sulfur dioxide: gas-phase oxidation by OH radicals and aqueous oxidation by H₂O₂, O₃ and iron catalysis, *Atmospheric Chemistry and Physics*, 12, 407-423, 2012b.
- Harris, E., Sinha, B., Van Pinxteren, D., Tilgner, A., Fomba, K. W., Schneider, J., Roth, A., Gnauk, T., Fahlbusch, B., and Mertes, S.: Enhanced role of transition metal ion catalysis during in-cloud oxidation of SO₂, *Science*, 340, 727-730, 2013a.
- 675 Harris, E., Sinha, B. r., Hoppe, P., and Ono, S.: High-precision measurements of ³³S and ³⁴S fractionation during SO₂ oxidation reveal causes of seasonality in SO₂ and sulfate isotopic composition, *Environmental science & technology*, 47, 12174-12183, 2013b.
- Hemingway, J., Olson, H., v Turchyn, A., Tipper, E., and Johnston, D. T.: Interpreting triple oxygen isotope signals from geologically preserved sulfate: Insights from modern Himalayan rivers, 2019.
- 680 Herrmann, H.: Kinetics of aqueous phase reactions relevant for atmospheric chemistry, *Chemical reviews*, 103, 4691-4716, 2003.
- Holt, B. and Kumar, R.: Oxygen isotope fractionation for understanding the sulphur cycle, *Stable Isotopes: Natural and Anthropogenic Sulphur in the Environment*. John Wiley & Sons, 1991. 27-41, 1991.
- 685 Holt, B. D., Cunningham, P. T., and Kumar, R.: Oxygen isotopy of atmospheric sulfates, *Environmental Science & Technology*, 15, 804-808, 1981.
- Janssen, C., Guenther, J., Krankowsky, D., and Mauersberger, K.: Relative formation rates of ⁵⁰O₃ and ⁵²O₃ in ¹⁶O–¹⁸O mixtures, *The Journal of chemical physics*, 111, 7179-7182, 1999.
- Jenkins, K. A. and Bao, H.: Multiple oxygen and sulfur isotope compositions of atmospheric sulfate in Baton Rouge, LA, USA, *Atmospheric Environment*, 40, 4528-4537, 2006.
- 690 Kampschulte, A. and Strauss, H.: The sulfur isotopic evolution of Phanerozoic seawater based on the analysis of structurally substituted sulfate in carbonates, *Chemical Geology*, 204, 255-286, 2004.
- Klemm, W. and Siedel, H.: Evaluation of the origin of sulphate compounds in building stone by sulphur isotope ratio, Geological Society, London, Special Publications, 205, 419-429, 2002.
- 695 Klimont, Z., Smith, S. J., and Cofala, J.: The last decade of global anthropogenic sulfur dioxide: 2000–2011 emissions, *Environmental Research Letters*, 8, 014003, 2013.
- Kloppmann, W., Bromblet, P., Vallet, J., Vergès-Belmin, V., Rolland, O., Guerrot, C., and Gosselin, C.: Building materials as intrinsic sources of sulphate: a hidden face of salt weathering of historical monuments investigated through multi-isotope tracing (B, O, S), *Science of the total environment*, 409, 1658-1669, 2011.
- 700 Kloppmann, W., Rolland, O., Proust, E., and Montech, A.: Soluble salt sources in medieval porous limestone sculptures: A multi-isotope (N, O, S) approach, *Science of the Total Environment*, 470, 559-566, 2014.
- Kramar, S., Mirtič, B., Knöller, K., and Rogan-Šmuc, N.: Weathering of the black limestone of historical monuments (Ljubljana, Slovenia): Oxygen and sulfur isotope composition of sulfate salts, *Applied geochemistry*, 26, 1632-1638, 2011.
- 705 Labidi, J., Cartigny, P., Birck, J., Assayag, N., and Bourrand, J.: Determination of multiple sulfur isotopes in glasses: A reappraisal of the MORB $\delta^{34}\text{S}$, *Chemical Geology*, 334, 189-198, 2012.
- Labidi, J., Cartigny, P., Hamelin, C., Moreira, M., and Dosso, L.: Sulfur isotope budget (³²S, ³³S, ³⁴S and ³⁶S) in Pacific–Antarctic ridge basalts: A record of mantle source heterogeneity and hydrothermal sulfide assimilation, *Geochimica et Cosmochimica Acta*, 133, 47-67, 2014.

- 710 Le Gendre, E., Martin, E., Villemant, B., Cartigny, P., and Assayag, N.: A simple and reliable anion-exchange resin method for sulfate extraction and purification suitable for multiple O-and S-isotope measurements, *Rapid Communications in Mass Spectrometry*, 31, 137-144, 2017.
- Lee, C.-W., Savarino, J., Cachier, H., and Thiemens, M.: Sulfur (^{32}S , ^{33}S , ^{34}S , ^{36}S) and oxygen (^{16}O , ^{17}O , ^{18}O) isotopic ratios of primary sulfate produced from combustion processes, *Tellus B: Chemical and Physical Meteorology*, 54, 193-200, 2002.
- 715 Lee, C. C. W. and Thiemens, M. H.: The $\delta^{17}\text{O}$ and $\delta^{18}\text{O}$ measurements of atmospheric sulfate from a coastal and high alpine region: A mass-independent isotopic anomaly, *Journal of Geophysical Research: Atmospheres*, 106, 17359-17373, 2001.
- 720 Li, L., Chen, Z., Zhang, Y., Zhu, T., Li, J., and Ding, J.: Kinetics and mechanism of heterogeneous oxidation of sulfur dioxide by ozone on surface of calcium carbonate, *Atmospheric Chemistry and Physics*, 6, 2453-2464, 2006.
- Li, X., Bao, H., Gan, Y., Zhou, A., and Liu, Y.: Multiple oxygen and sulfur isotope compositions of secondary atmospheric sulfate in a mega-city in central China, *Atmospheric environment*, 81, 591-599, 2013.
- Lin, Y., Sim, M., and Ono, S.: Multiple-sulfur isotope effects during photolysis of carbonyl sulfide, 2011. 2011.
- 725 Lin, M., Kang, S., Shaheen, R., Li, C., Hsu, S.-C., and Thiemens, M. H.: Atmospheric sulfur isotopic anomalies recorded at Mt. Everest across the Anthropocene, *Proceedings of the National Academy of Sciences*, 115, 6964-6969, 2018a.
- Lin, M., Zhang, X., Li, M., Xu, Y., Zhang, Z., Tao, J., Su, B., Liu, L., Shen, Y., and Thiemens, M. H.: Five-S-isotope evidence of two distinct mass-independent sulfur isotope effects and implications for the modern and Archean atmospheres, *Proceedings of the National Academy of Sciences*, 115, 8541-8546, 2018b.
- 730 Lloyd, R.: Oxygen isotope behavior in the sulfate-water system, *Journal of Geophysical Research*, 73, 6099-6110, 1968.
- Longinelli, A. and Bartelloni, M.: Atmospheric pollution in Venice, Italy, as indicated by isotopic analyses, *Water, Air, and Soil Pollution*, 10, 335-341, 1978.
- 735 Lyons, J. R.: Transfer of mass-independent fractionation in ozone to other oxygen-containing radicals in the atmosphere, *Geophysical Research Letters*, 28, 3231-3234, 2001.
- Markovic, S., Paytan, A., Li, H., and Wortmann, U. G.: A revised seawater sulfate oxygen isotope record for the last 4 Myr, *Geochimica et Cosmochimica Acta*, 175, 239-251, 2016.
- Martin, E., Bekki, S., Ninin, C., and Bindeman, I.: Volcanic sulfate aerosol formation in the troposphere, *Journal of Geophysical Research: Atmospheres*, 119, 6600-6612, 2014.
- 740 Martin, E.: Volcanic plume impact on the atmosphere and climate: O-and S-isotope insight into sulfate aerosol formation, *Geosciences*, 8, 198, 2018.
- Mauersberger, K., Erbacher, B., Krankowsky, D., Günther, J., and Nickel, R.: Ozone isotope enrichment: Isotopomer-specific rate coefficients, *Science*, 283, 370-372, 1999.
- 745 Montana, G., Randazzo, L., and Mazzoleni, P.: Natural and anthropogenic sources of total suspended particulate and their contribution to the formation of black crusts on building stone materials of Catania (Sicily), *Environmental Earth Sciences*, 67, 1097-1110, 2012.
- Montana, G., Randazzo, L., Oddo, I. A., and Valenza, M.: The growth of "black crusts" on calcareous building stones in Palermo (Sicily): a first appraisal of anthropogenic and natural sulphur sources, *Environmental geology*, 56, 367-380, 2008.
- 750 Nielsen, H.: Isotopic composition of the major contributors to atmospheric sulfur, *Tellus*, 26, 213-221, 1974.
- Oduro, H., Harms, B., Sintim, H. O., Kaufman, A. J., Cody, G., and Farquhar, J.: Evidence of magnetic isotope effects during thermochemical sulfate reduction, *Proceedings of the National Academy of Sciences*, 108, 17635-17638, 2011.
- 755 Ono, S., Eigenbrode, J. L., Pavlov, A. A., Kharecha, P., Rumble III, D., Kasting, J. F., and Freeman, K. H.: New insights into Archean sulfur cycle from mass-independent sulfur isotope records from the Hamersley Basin, Australia, *Earth and Planetary Science Letters*, 213, 15-30, 2003.
- Ono, S., Whitehill, A., and Lyons, J.: Contribution of isotopologue self-shielding to sulfur mass-independent fractionation during sulfur dioxide photolysis, *Journal of Geophysical Research: Atmospheres*, 118, 2444-2454, 2013.
- 760 Ono, S., Wing, B., Johnston, D., Farquhar, J., and Rumble, D.: Mass-dependent fractionation of quadruple stable sulfur isotope system as a new tracer of sulfur biogeochemical cycles, *Geochimica et Cosmochimica Acta*, 70, 2238-2252, 2006a.
- 765 Ono, S., Wing, B., Rumble, D., and Farquhar, J.: High precision analysis of all four stable isotopes of sulfur (^{32}S , ^{33}S , ^{34}S and ^{36}S) at nanomole levels using a laser fluorination isotope-ratio-monitoring gas chromatography - mass spectrometry, *Chemical geology*, 225, 30-39, 2006b.

- Patris, N., Delmas, R., Legrand, M., De Angelis, M., Ferron, F. A., Stiévenard, M., and Jouzel, J.: First sulfur isotope measurements in central Greenland ice cores along the preindustrial and industrial periods, *Journal of Geophysical Research: Atmospheres*, 107, ACH 6-1-ACH 6-11, 2002.
- 770 Raab, M. and Spiro, B.: Sulfur isotopic variations during seawater evaporation with fractional crystallization, *Chemical Geology: Isotope Geoscience section*, 86, 323-333, 1991.
- Rees, C., Jenkins, W., and Monster, J.: The sulphur isotopic composition of ocean water sulphate, *Geochimica et Cosmochimica Acta*, 42, 377-381, 1978.
- Rennie, V. C. and Turchyn, A. V.: The preservation of $\delta\text{SSO}434$ and $\delta\text{OSO}418$ in carbonate-associated sulfate during marine diagenesis: A 25 Myr test case using marine sediments, *Earth and Planetary Science Letters*, 395, 13-23, 2014.
- 775 Rodriguez-Navarro, C. and Sebastian, E.: Role of particulate matter from vehicle exhaust on porous building stones (limestone) sulfation, *Science of the total environment*, 187, 79-91, 1996.
- Romero, A. B. and Thiemens, M. H.: Mass-independent sulfur isotopic compositions in present-day sulfate aerosols, *Journal of Geophysical Research: Atmospheres*, 108, 2003.
- 780 Sáiz-Jiménez, C.: Deposition of anthropogenic compounds on monuments and their effect on airborne microorganisms, *Aerobiologia*, 11, 161-175, 1995.
- Savarino, J., Lee, C. C., and Thiemens, M. H.: Laboratory oxygen isotopic study of sulfur (IV) oxidation: Origin of the mass-independent oxygen isotopic anomaly in atmospheric sulfates and sulfate mineral deposits on Earth, *Journal of Geophysical Research: Atmospheres*, 105, 29079-29088, 2000.
- 785 Savarino, J. and Thiemens, M. H.: Analytical procedure to determine both $\delta^{18}\text{O}$ and $\delta^{17}\text{O}$ of H_2O_2 in natural water and first measurements, *Atmospheric Environment*, 33, 3683-3690, 1999.
- Scheerer, S., Ortega-Morales, O., and Gaylarde, C.: Microbial Deterioration of Stone Monuments—An Updated Overview, 66, 97-139, 2009.
- Schiavon, N.: Biodeterioration of calcareous and granitic building stones in urban environments, *Geological Society, London, Special Publications*, 205, 195-205, 2002.
- 790 Seinfeld, J. H. and Pandis, S. N.: Atmospheric chemistry and physics: from air pollution to climate change, John Wiley & Sons, 2016.
- Shaheen, R., Abaunza, M. M., Jackson, T. L., McCabe, J., Savarino, J., and Thiemens, M. H.: Large sulfur-isotope anomaly in nonvolcanic sulfate aerosol and its implications for the Archean atmosphere, *Proceedings of the National Academy of Sciences*, 111, 11979-11983, 2014.
- 795 Siegesmund, S., Török, A., Hüper, A., Müller, C., and Klemm, W.: Mineralogical, geochemical and microfabric evidences of gypsum crusts: a case study from Budapest, *Environmental Geology*, 52, 385-397, 2007.
- Sofen, E., Alexander, B., and Kunasek, S.: The impact of anthropogenic emissions on atmospheric sulfate production pathways, oxidants, and ice core $\Delta^{17}\text{O}(\text{SO}_4^{2-})$, *Atmospheric Chemistry and Physics*, 11, 3565-3578, 2011.
- 800 Šrámek, J.: Determination of the source of surface deterioration on tombstones at the Old Jewish Cemetery in Prague, *Studies in Conservation*, 25, 47-52, 1980.
- Stocker, T.: Climate change 2013: the physical science basis: Working Group I contribution to the Fifth assessment report of the Intergovernmental Panel on Climate Change, Cambridge University Press, 2014.
- 805 Thiemens, M. H.: Mass-independent isotope effects in planetary atmospheres and the early solar system, *Science*, 283, 341-345, 1999.
- Thode, H., Monster, J., and Dunford, H.: Sulphur isotope geochemistry, *Geochimica et Cosmochimica Acta*, 25, 159-174, 1961.
- Thomazo, C., Brayard, A., Elmeknassi, S., Vennin, E., Olivier, N., Caravaca, G., Escarguel, G., Fara, E., Bylund, K., and Jenks, J.: Multiple sulfur isotope signals associated with the late Smithian event and the Smithian/Spathian boundary, *Earth-Science Reviews*, 2018, 2018.
- 810 Thurston, R. S., Mandernack, K. W., and Shanks III, W. C.: Laboratory chalcopyrite oxidation by *Acidithiobacillus ferrooxidans*: oxygen and sulfur isotope fractionation, *Chemical Geology*, 269, 252-261, 2010.
- Tiano, P.: Biodegradation of cultural heritage: decay mechanisms and control methods, 2002, 7-12.
- 815 Tiano, P., Bianchi, R., Gargani, G., and Vannucci, S.: Research on the presence of sulphurcycle bacteria in the stone of some historical buildings in Florence, *Plant and soil*, 43, 211-217, 1975.
- Torfs, K. M., Van Grieken, R. E., and Buzek, F.: Use of stable isotope measurements to evaluate the origin of sulfur in gypsum layers on limestone buildings, *Environmental science & technology*, 31, 2650-2655, 1997.
- Turchyn, A. V., Schrag, D. P., Coccioni, R., and Montanari, A.: Stable isotope analysis of the Cretaceous sulfur cycle, *Earth and Planetary Science Letters*, 285, 115-123, 2009.
- 820 Turro, N. J.: Influence of nuclear spin on chemical reactions: magnetic isotope and magnetic field effects (a review), *Proceedings of the National Academy of Sciences*, 80, 609-621, 1983.

- Urey, H. C.: The thermodynamic properties of isotopic substances, *Journal of the Chemical Society (Resumed)*, 1947. 562-581, 1947.
- 825 Vallet, J.-M., Gosselin, C., Bromblet, P., Rolland, O., Vergès-Belmin, V., and Kloppmann, W.: Origin of salts in stone monument degradation using sulphur and oxygen isotopes: First results of the Bourges cathedral (France), *Journal of geochemical exploration*, 88, 358-362, 2006.
- Vicars, W. C. and Savarino, J.: Quantitative constraints on the $\delta^{17}\text{O}$ -excess ($\Delta^{17}\text{O}$) signature of surface ozone: Ambient measurements from 50° N to 50° S using the nitrite-coated filter technique, *Geochimica et*
- 830 *Cosmochimica Acta*, 135, 270-287, 2014.
- Weber, R., Chen, G., Davis, D., Mauldin III, R., Tanner, D., Eisele, F., Clarke, A., Thornton, D., and Bandy, A.: Measurements of enhanced H_2SO_4 and 3–4 nm particles near a frontal cloud during the First Aerosol Characterization Experiment (ACE 1), *Journal of Geophysical Research: Atmospheres*, 106, 24107-24117, 2001.
- 835 Young, E. D., Galy, A., and Nagahara, H.: Kinetic and equilibrium mass-dependent isotope fractionation laws in nature and their geochemical and cosmochemical significance, *Geochimica et Cosmochimica Acta*, 66, 1095-1104, 2002.

840

845

850

855



Fig. 1 Thin layer of black crusts formed on a carbonate building stone, on a church wall in Fécamp city.

860

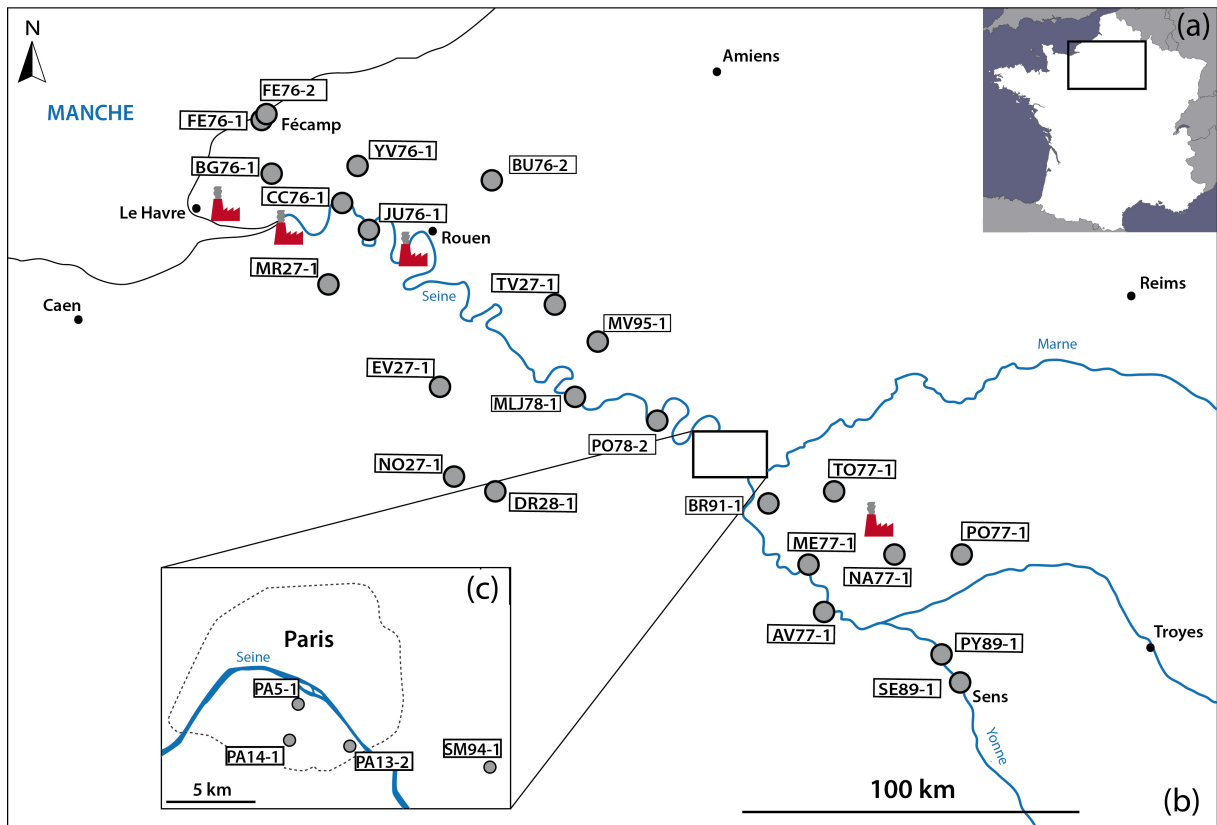


Fig. 2 Maps with the sampling location. **a** Location of the studied area in the Northern Paris Basin on the map of France. **b** The NW-SE cross-section from Fécamp to Sens with the 27 samples and the four power plants (in red). **c** Focus on the samples located in the Paris area.

865

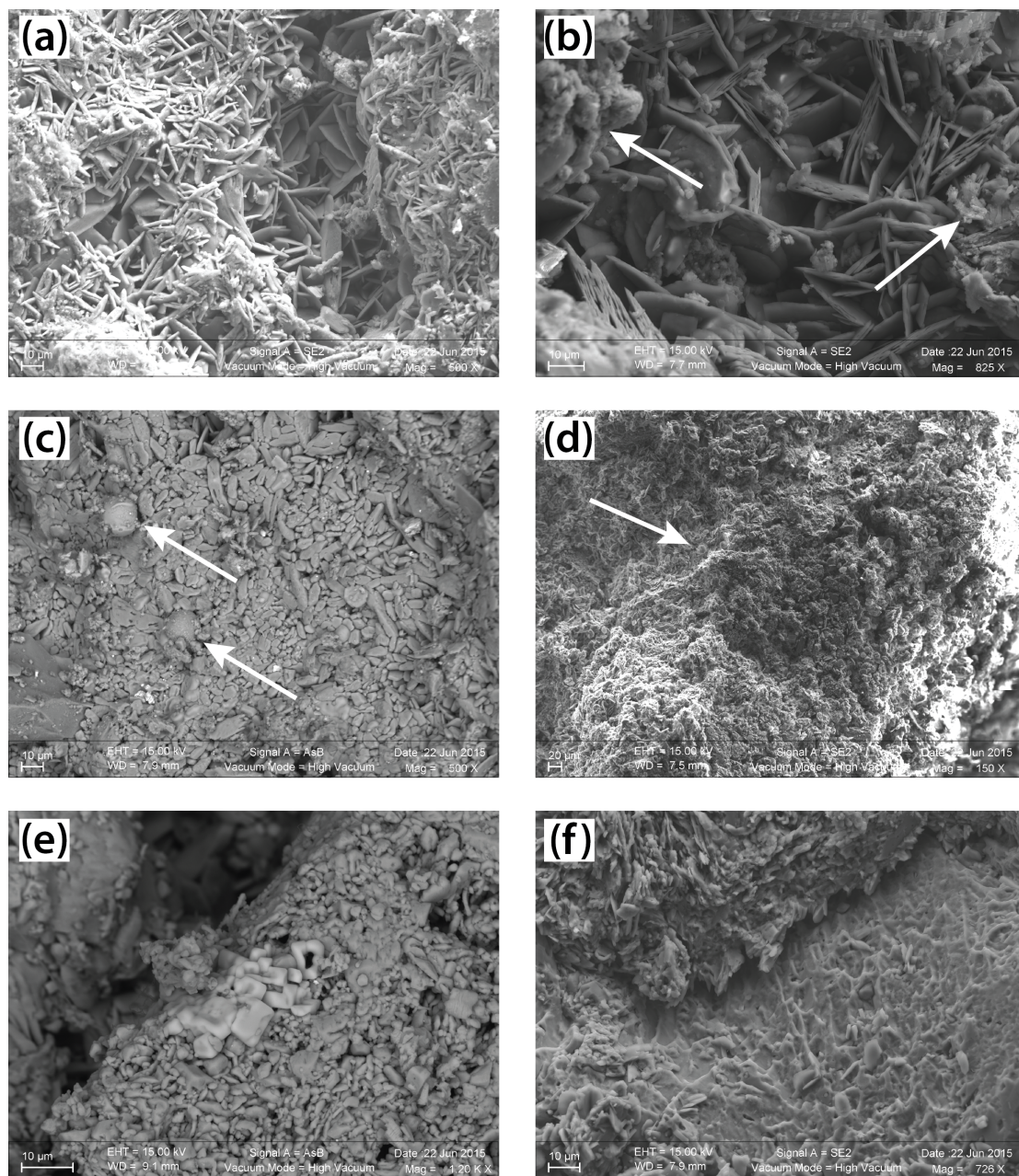


Fig. 3 SEM images of black crusts samples from Paris (PA14-1, PA13-2) and Montfort-sur-Risles (MR27-1). **a** Two distinct layers into the crust: an upper opaque one with aggregates of particulate matter and clay minerals (left and right sides of the picture) and a more crystallized one with acicular gypsum crystals perpendicular to the host substrate. **b** Presence of soot (arrow) on the two layers (PA14-1). **c** Fly ashes (arrow) with the formation of small gypsum crystals on their surfaces (PA13-2). **d** Large amount of fly ashes (arrow and smaller not indicated) and soot in MR27-1 sample, located in a rural place. **e** Isolated cubic crystals of halite (NaCl) in MR27-1 sample, at 28 km from the coastline. **f** Dissolution of the underlying limestone (on the bottom) and subsequently the precipitation of gypsum (on the top).

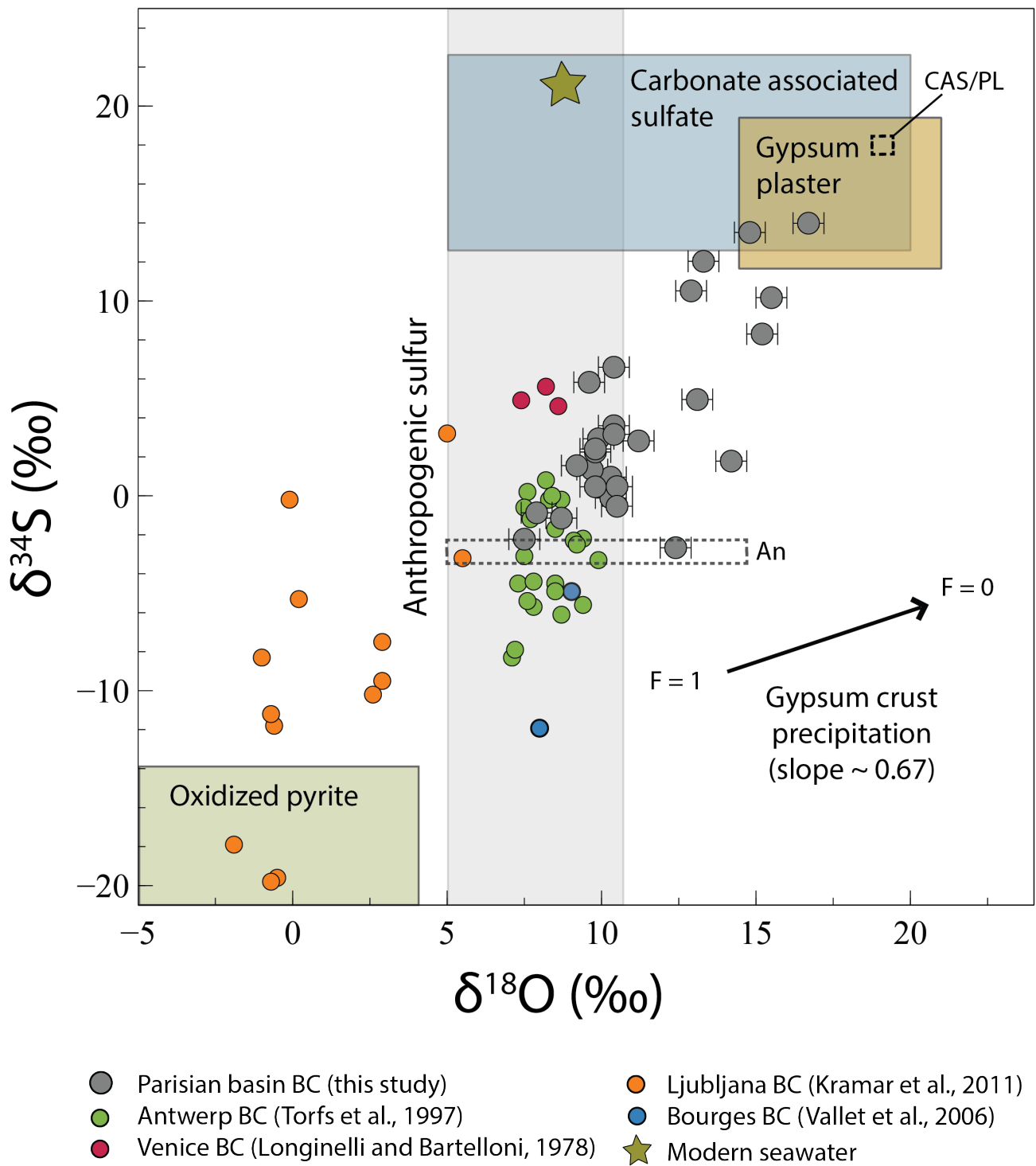
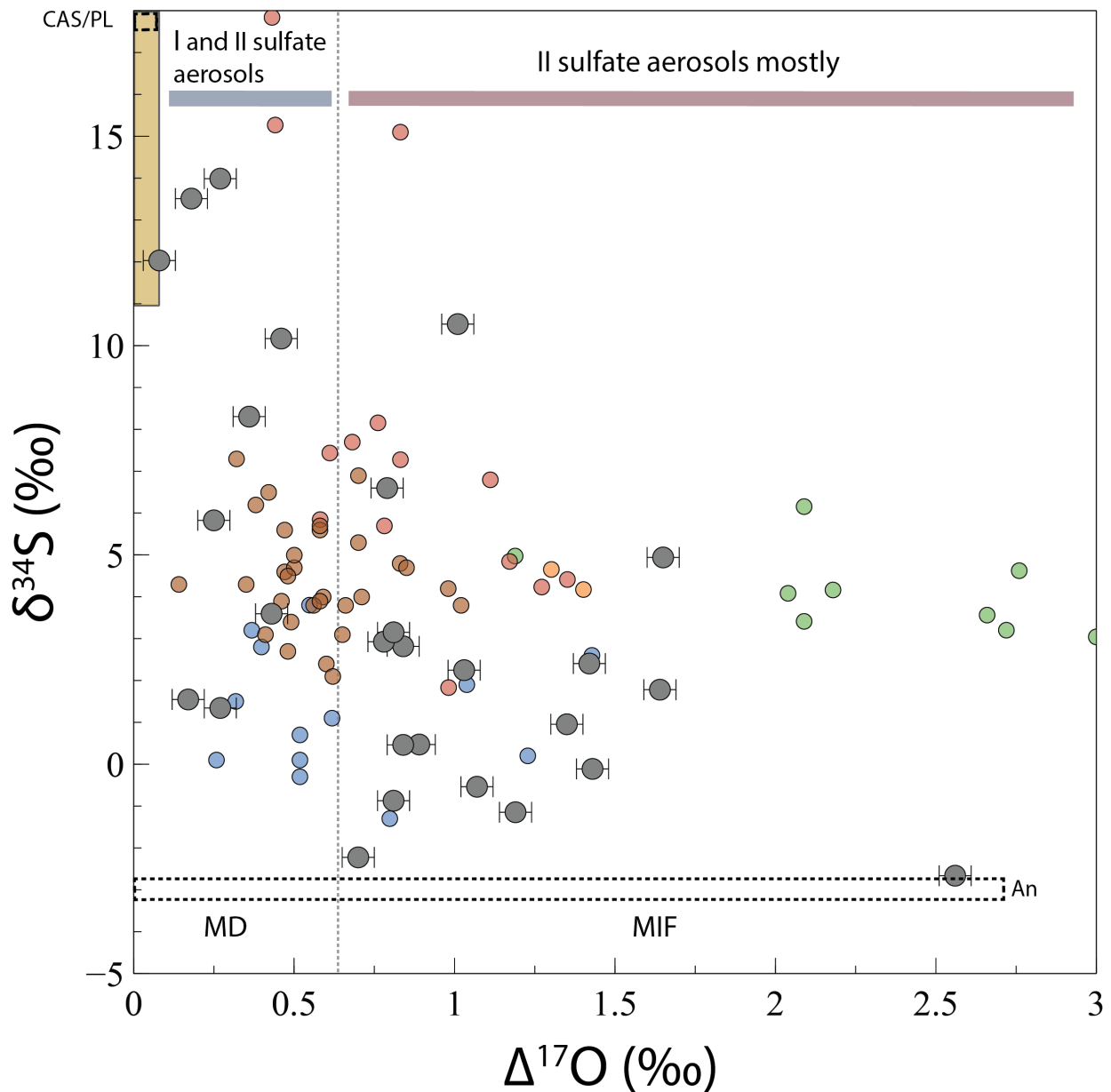


Fig. 4 Evolution of $\delta^{34}\text{S}$ with $\delta^{18}\text{O}$ in black crusts (BC) sulfates. Modern seawater $\delta^{18}\text{O}$ and $\delta^{34}\text{S}$ are from Markovic et al., (2016) and Rees et al., (1978) respectively. The extreme anthropogenic sulfate $\delta^{18}\text{O}$ and $\delta^{34}\text{S}$ are from Lee et al. (2002) and Faure (1986) respectively. The carbonate-associated sulfates compositions are from Rennie and Turchyn, (2014) and Turchyn et al., (2009) and those of gypsum plaster come from Kloppmann et al., (2011). Isotopic compositions determining the oxidized pyrite field is from Canfield (2004) for sulfur and is calculated following a Rayleigh distillation model with an initial H_2O $\delta^{18}\text{O} = 6\text{‰}$ and a mean fractionation factor of 1.010 (Gomes and Johnston, 2017) for oxygen. The black arrow represents the fractionation induced by gypsum precipitation where $F=1$ mean that all sulfates are dissolved and $F=0$ means that all sulfates are precipitated. The dashed fields represent the sulfur isotopic composition of the two anthropogenic (An) and CAS/plaster (CAS/PL) end-members.



- Parisian basin BC (this study)
- Baton Rouge SA (Jenkins and Bao, 2006)
- Wuhan SA (Li et al., 2013)
- Bakersfield SA (Bao et al., 2001; Romero and Thiemens, 2003)
- La Jolla SA (Lee and Thiemens, 2001; Romero and Thiemens, 2003)
- WMRS SA (Lee and Thiemens, 2001; Romero and Thiemens, 2003)

895

Fig. 5 Evolution of $\delta^{34}\text{S}$ with $\Delta^{17}\text{O}$ in black crusts (BC) sulfates and sulfate aerosols (SA). The limit between mass-dependent and mass-independent fractionation (dashed line) is defined for $\Delta^{17}\text{O} \sim 0.65$ ‰, where H_2O_2 will be the major oxidant, giving its O-anomaly to sulfates (Savarino et al., 2000). When $\Delta^{17}\text{O} < 0.65$ ‰, black crusts sulfates result from a mixing between primary sulfates (gypsum plaster and CAS and/or anthropogenic sulfur) and secondary sulfate aerosols where SO_2 is oxidized by H_2O_2 ($\Delta^{17}\text{O} = 0.65$ ‰), OH ($\Delta^{17}\text{O} = 0$ ‰) or O_2 -TMI ($\Delta^{17}\text{O} = -0.09$ ‰) mainly (grey bar). When $\Delta^{17}\text{O} > 0.65$ ‰, black crusts sulfates represent secondary sulfate aerosols mainly, resulting from a mixing between SO_2 oxidized by O_3 ($\Delta^{17}\text{O} = 8.75$ ‰) and H_2O_2 (red bar). The yellow array represents gypsum plaster and CAS isotopic compositions. The dashed fields represent the sulfur isotopic composition of the two anthropogenic (An) and CAS/plaster (CAS/PL) end-members.

900

905

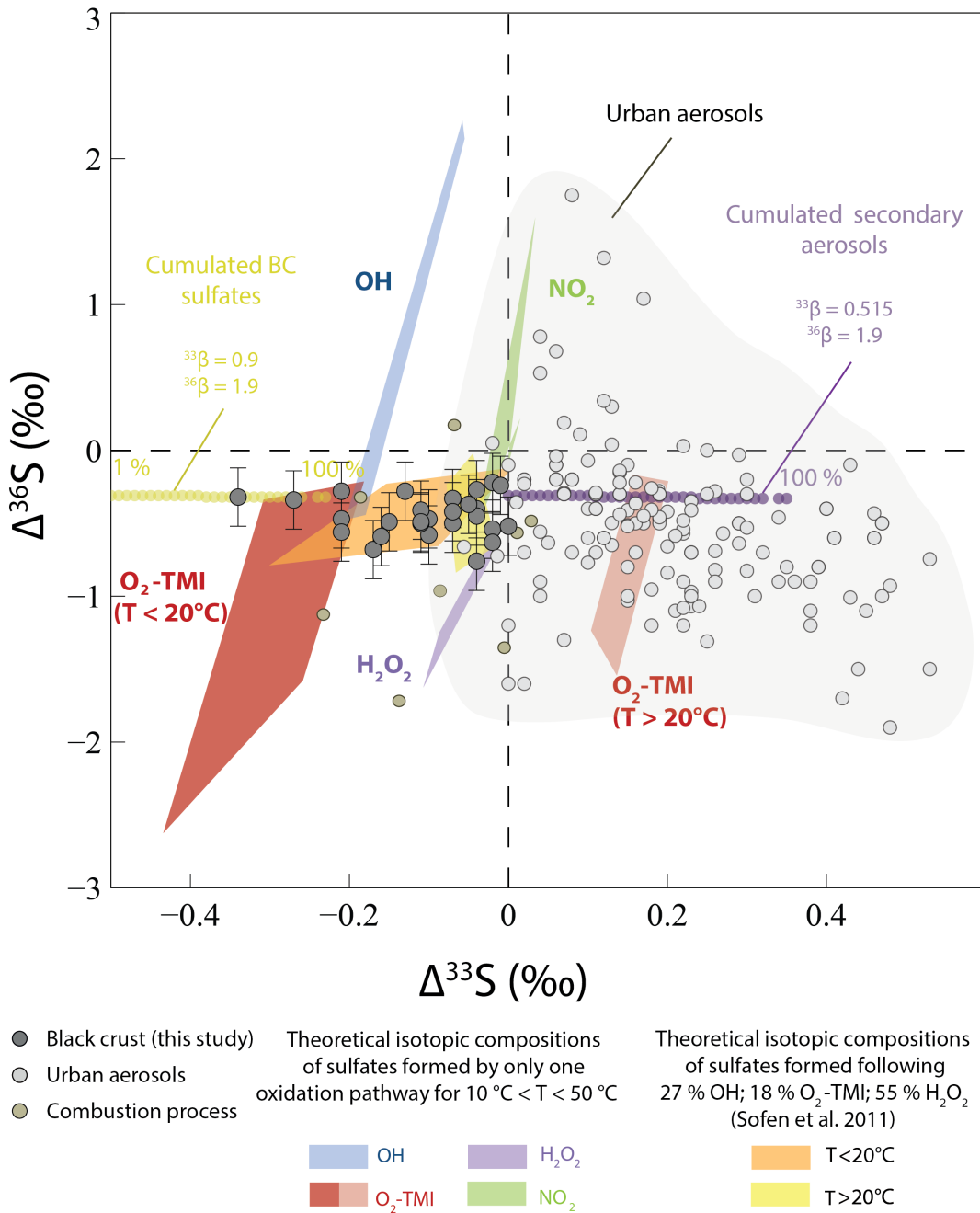
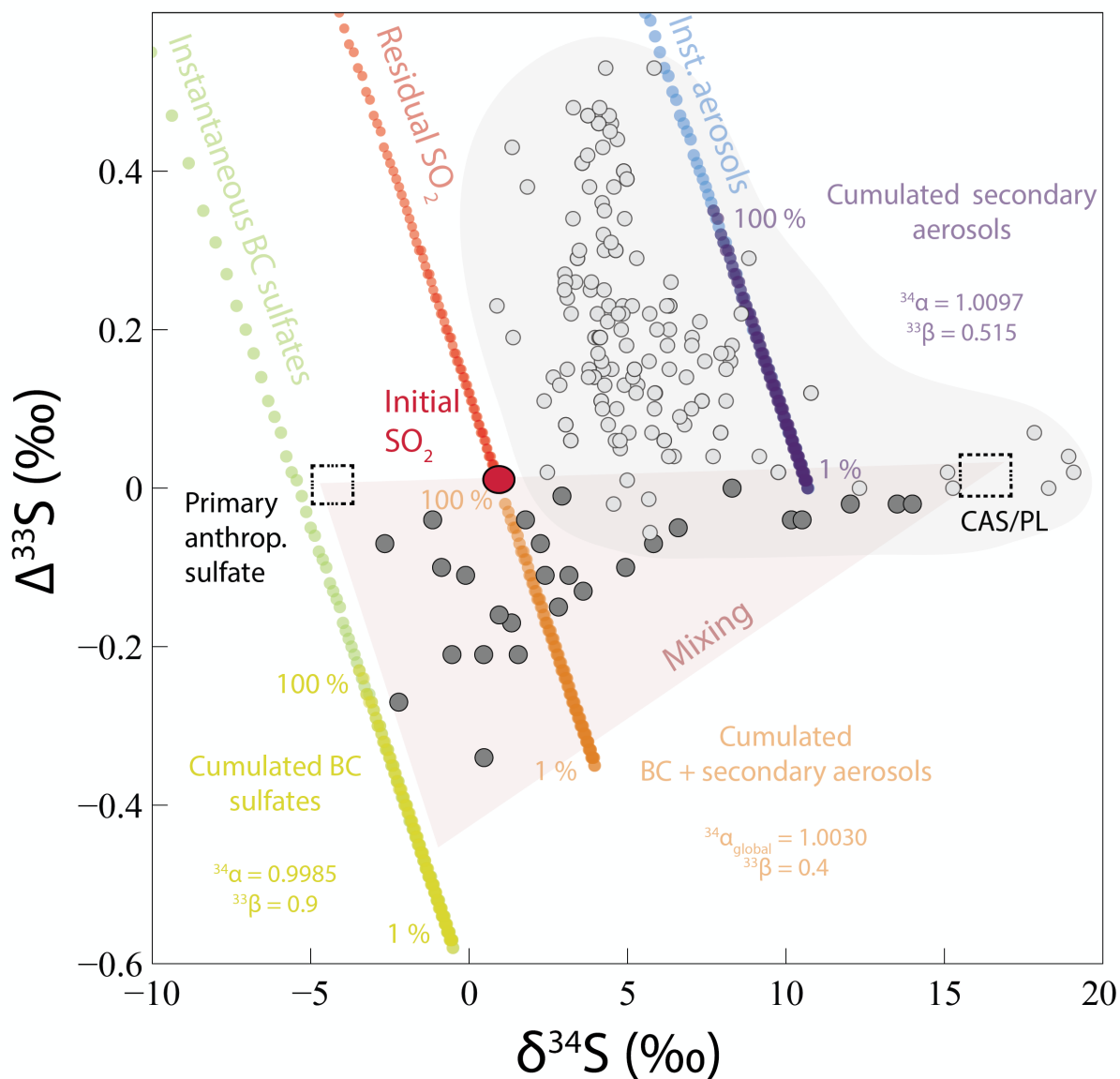


Fig. 6 $\Delta^{33}\text{S}$ and $\Delta^{36}\text{S}$ of the black crust, compared to sulfates formed by different oxidation pathways and by a mixing of them in the proportions estimated by Sofen et al. (2011). We took $^{33}\beta_{\text{H}_2\text{O}_2/\text{O}_3} = 0.511$, $^{33}\beta_{\text{OH}} = 0.503$, $^{33}\beta_{\text{O}_2\text{-TMI}} = 0.498$ (for $T < 20^\circ\text{C}$), $^{33}\beta_{\text{O}_2\text{-TMI}} = 0.547$ (for $T > 20^\circ\text{C}$), $^{33}\beta_{\text{NO}_2} = 0.514$ and $^{36}\beta_{\text{H}_2\text{O}_2/\text{O}_3} = 1.82$, $^{36}\beta_{\text{OH}} = 1.97$, $^{36}\beta_{\text{O}_2\text{-TMI}} = 1.98$ (for $T < 20^\circ\text{C}$ and $T > 20^\circ\text{C}$), and $^{36}\beta_{\text{NO}_2} = 1.90$ (Au Yang et al., 2018; Harris et al., 2013b). As $^{33}\beta_{\text{O}_3}$ and $^{36}\beta_{\text{O}_3}$ are unknown, we modified the proportions of Sofen et al. (2011) as follows: 27 % OH, 18 % O₂-TMI, 55 % H₂O₂ and 0 % O₃. The urban aerosols isotopic compositions are a compilation from Au Yang et al. (2019); Guo et al. (2010); (Lin et al., 2018b); Romero and Thiemens (2003); Shaheen et al. (2014) while the combustion process reflect samples from (Lee et al., 2002). Modeled $\Delta^{33}\text{S}$ - $\Delta^{36}\text{S}$ -values of cumulated black crusts (BC) sulfates formed by SO₂ wet/dry deposition with a MIE (^{33}S -depletion compared to initial SO₂ with constant negative $\Delta^{36}\text{S}$) and of cumulated secondary aerosols formed by SO₂ oxidation by O₃, O₂-TMI, OH, H₂O₂ (^{33}S -enrichment compared to initial SO₂) from an initial SO₂ with $\Delta^{33}\text{S}$ - $\Delta^{36}\text{S} = 0$ ‰ are reported with corresponding β exponents (see section 5.2.2 for model explanation). Residual SO₂ and global cumulated BC + secondary aerosols isotopic compositions were not reported for better readability. Percentages indicate the fraction of produced cumulated BC and secondary aerosols.

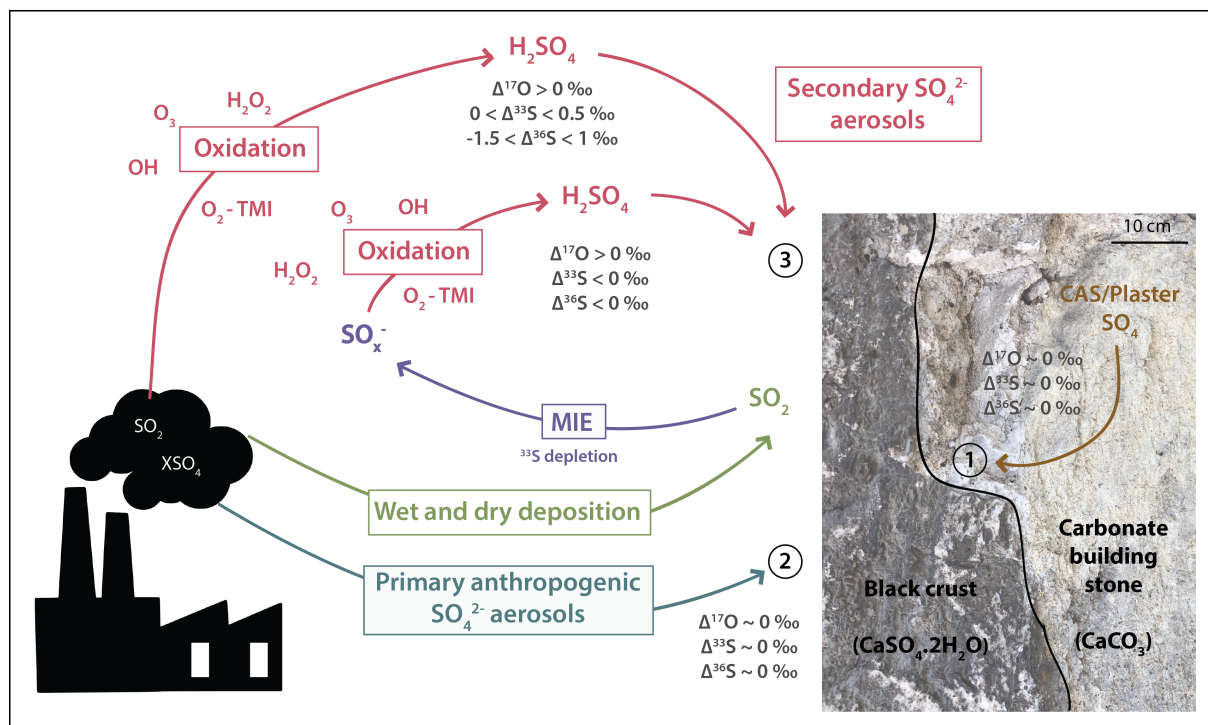


925 **Fig. 7 a** Modeled $\delta^{34}\text{S}$ and $\Delta^{33}\text{S}$ -values of black crusts (BC) sulfates (instantaneous and cumulated) formed by SO_2 wet/dry deposition with a MIE (^{33}S -depletion compared to initial SO_2) and of secondary aerosols (instantaneous and cumulated) formed by SO_2 oxidation by O_3 , O_2 -TMI, OH , H_2O_2 (^{33}S -enrichment compared to initial SO_2) from an initial SO_2 with $\delta^{34}\text{S} = 1 \text{ ‰}$ and $\Delta^{33}\text{S} = 0 \text{ ‰}$ (red point). ^{33}S -enrichment of residual SO_2 and global cumulated BC + secondary aerosols isotopic compositions are also reported. Percentages indicate the fraction of produced cumulated BC and secondary aerosols (see section 5.2.2 for model explanation). Black crust sulfate isotopic compositions (dark grey points) can be explained by a mixing (red triangle) between sulfates from CAS/plaster (dashed square, $\delta^{34}\text{S} = 18 \text{ ‰}$ and $\Delta^{33}\text{S} = 0 \text{ ‰}$, see section 5.1), primary anthropogenic sulfates (dashed square, $\delta^{34}\text{S} = -3 \text{ ‰}$ and $\Delta^{33}\text{S} = 0 \text{ ‰}$) and sulfates formed by wet/dry deposition of SO_2 undergoing a MIE and oxidized SO_2 forming secondary aerosols (cumulated BC sulfates and cumulated BC + secondary aerosols). Urban aerosols (light grey points) isotopic compositions are a compilation from Au Yang et al. (2019); Guo et al. (2010); (Lin et al., 2018b); Romero and Thiemens (2003); Shaheen et al. (2014).

930

935

940



945 **Fig. 8** Scheme summarizing the sulfur sources and processes that lead to black crusts formation. Sulfur dioxide releases by anthropogenic activities can either be oxidized in the atmosphere by H_2O_2 , O_3 , OH , O_2 -TMI and formed secondary sulfate aerosols that will react with the carbonate building stone to produce ^{33}S -enriched black crusts sulfates or be deposited, as dry/wet deposit, on the carbonate substrate where its oxidation into SO_x^- then sulfates through MIE will produce ^{33}S -depleted black crusts sulfates and a ^{33}S -enriched residual SO_2 (source 3).
 950 Primary sulfates emitted by anthropogenic activities (source 2) or carbonate-associated sulfates and/or plaster of the host-rock (source 1) are also likely sources contributing to black crusts formation.

955

960

965

Samples	Location	Orientation of sampled faces	Distance from the sea (km)	Height above the ground (m)	Exposition to traffic road
PA14-1	48° 49' 37.97" N 2° 20' 5.21" E	65° N	170	1.5 - 2.0	Directly exposed
PA13-2	48° 49' 26.42" N 2° 22' 33.48" E	150° N	170	2.0	Directly exposed
PA5-1	48° 50' 37.09" N 2° 20' 25.77" E	14° N	170	1.5	Directly exposed
BR91-1	48° 42' 11.15" N 2° 30' 28.82" E	107° N	190	1.5	Directly exposed
PO78-2	48° 55' 42.41" N 2° 2' 16.94" E	100° N	150	1.5 - 2.0	Directly exposed
MLJ78-1	48° 59' 32.40" N 1° 42' 31.78" E	295° N	135	1.2 - 1.5	Directly exposed
SM94-1	48° 48' 47.00" N 2° 28' 28.84" E	0° N	175	2.0 - 3.5	Directly exposed
TO77-1	48° 44' 18.74" N 2° 46' 7.78" E	21° N	202	1.5 – 2.0	Directly exposed
MV95-1	49° 9' 3.57" N 1° 47' 13.53" E	343° N	110	1.5	Not directly exposed
TV27-1	49° 14' 8.17" N 1° 36' 27.30" E	340° N	95	1.5 – 2.0	Directly exposed
BU76-2	49° 35' 2.94" N 1° 21' 23.79" E	313° N	45	1.5 – 2.0	Directly exposed
YV76-1	49° 37' 1.12" N 0° 45' 16.36" E	275° N	28	1.5 – 2.0	Not directly exposed
FE76-1	49° 45' 31.47" N 0° 22' 2.74" E	190° N	0,5	1.5 – 2.0	Directly exposed
FE76-2	49° 45' 29.26" N 0° 22' 35.97" E	0° N	1,1	1.5 – 2.0	Not directly exposed
BG76-1	49° 35' 30.11" N 0° 25' 39.22" E	151° N	21	1.5	Not directly exposed
CC76-1	49° 31' 32.55" N 0° 43' 50.12" E	191° N	37	< 2.0	Directly exposed
JU76-1	49° 25' 56.69" N 0° 49' 8.42" E	317° N	50	1.5 – 2.0	Directly exposed
MR27-1	49° 17' 40.51" N 0° 39' 52.77" E	120° N	28	< 2.0	Directly exposed
EV27-1	49° 1' 25.82" N 1° 8' 29.45" E	158° N	84	2.0	Not directly exposed
NO27-1	48° 46' 15.78" N 1° 11' 53.81" E	13° N	103	1.5	Not directly exposed
DR28-1	48° 44' 9.39" N 1° 22' 5.06" E	233° N	115	1.5 – 2.0	Not directly exposed

ME77-2	48° 32' 20'' N 2° 39' 33 '' E	22° N	210	1.3	Not directly exposed
AV77-1	48° 24' 15 '' N 2° 43' 2'' E	73° N	230	1.3 – 2.3	Directly exposed
SE89-1	48° 12' 8'' N 3° 16' 24'' E	263° N	270	1.7	Not directly exposed
PY89-1	48° 17' 16'' N 3° 12' 16'' E	343° N	263	1.5 – 2.1	Not directly exposed
PO77-1	48° 33' 38'' N 3° 17' 29'' E	23° N	230	1.5 – 2.0	Not directly exposed
NA77-1	48° 33' 26'' N 3° 0' 25'' E	351° N	230	2.5	Not directly exposed

Table 1 Characteristics of black crusts samples. Their name was given according to the city and the department where they are located and following the number of samples gathered at the same place (NA77-1: NA = Nangis; 77 = department; -1 = first sample collected).

975

980

985

990

995

000

	$\delta^{18}\text{O}$	$\Delta^{17}\text{O}$	$\delta^{34}\text{S}$	$\Delta^{33}\text{S}$	$\Delta^{36}\text{S}$	Distance from
(2 σ)	$\pm 0.5 \text{ ‰}$	$\pm 0.05 \text{ ‰}$	$\pm 0.20 \text{ ‰}$	$\pm 0.01 \text{ ‰}$	$\pm 0.20 \text{ ‰}$	coastline (km)
PO78-2	9.7	0.27	1.34	-0.17	-0.68	150
AV77-1	9.8	1.03	2.25	-0.07	-0.33	230
PY89-1	9.8	0.84	0.46	-0.21	-0.47	263
PO77-1	12.4	2.56	-2.66	-0.07	-0.50	231
BG76-1	13.1	1.65	4.94	-0.10	-0.47	21
MV95-1	15.5	0.46	10.17	-0.04	-0.40	110
BR91-1	14.8	0.18	13.51	-0.02	-0.22	190
JU76-1	9.9	0.78	2.93	-0.01	-0.24	50
TV27-1	16.7	0.27	13.99	-0.02	-0.54	95
YV76-1	12.9	1.01	10.51	-0.04	-0.27	28
DR28-1	7.5	0.70	-2.22	-0.30	-0.34	115
FE76-1	10.3	1.35	0.95	-0.16	-0.59	0.5
NO27-1	14.2	1.64	1.78	-0.04	-0.45	103
ME77-2	10.5	1.07	-0.54	-0.21	-0.29	210
PA13-2	7.9	0.81	-0.87	-0.10	-0.58	170
MLJ78-1	15.2	0.36	8.30	0.00	-0.52	135
EV27-1	10.4	0.79	6.60	-0.05	-0.37	84
FE76-2	8.7	1.19	-1.15	-0.04	-0.76	1.1
SE89-1	10.4	0.81	3.15	-0.11	-0.41	270
BU76-2	10.3	1.43	-0.11	-0.11	-0.50	45
MR27-1	11.2	0.84	2.82	-0.15	-0.49	28
PA14-1	9.2	0.17	1.55	-0.21	-0.56	171
TO77-1	13.3	0.08	12.03	-0.02	-0.64	202
NA77-1	9.8	1.42	2.40	-0.11	-0.49	232
PA5-1	10.5	0.89	0.47	-0.34	-0.32	172
SM94-1	10.4	0.43	3.60	-0.13	-0.28	175
CC76-1	9.6	0.25	5.82	-0.07	-0.43	37

Table 2 $\delta^{18}\text{O}$, $\delta^{34}\text{S}$, $\Delta^{17}\text{O}$, $\Delta^{33}\text{S}$ and $\Delta^{36}\text{S}$ measures of each sample with the distance from coastline.

005